A sea surface temperature reconstruction for the southern Indian Ocean trade wind belt from corals in Rodrigues Island (19°S, 63°E)

J. Zinke[1,2,3,4], L. Reuning[5], M. Pfeiffer[5], J. Wassenburg[6], E. Hardman[7], R. Jhangeer-Khan[7], Davies, G. R.[8], C.K.C. Ng[9], and D. Kroon[10]

[1]Department of Environment and Agriculture, Curtin University of Technology, Kent Street, Bentley, WA6102, Australia

[2]Division of Paleontology, Freie Universitaet Berlin, Malteserstrasse 74-100, Berlin, 12249, Germany

[3]Australian Institute of Marine Science, Nedlands, WA 6009, Australia

[4]School of Geography, Archaeology and Environmental Studies, University of Witwatersrand, Johannesburg, South Africa.

[5]Geological Institute, RWTH Aachen, Wuellnerstrasse2, 52056 Aachen, Germany

[6]Institute for Geosciences, Johannes-Gutenberg-University Mainz, Johann-Joachim-Becher-Weg 21, D-55128 Mainz

[7]SHOALS Rodrigues, Rodrigues, Mauritius

[8]Geology & Geochemistry, VU University Amsterdam, De Boelelaan 1085, 1081 HV Amsterdam, Netherlands

[9]Department of Medical Radiation Sciences, Curtin University of Technology, Kent Street, Bentley, WA6102, Australia

[10]University of Edinburgh, School of GeoSciences, The King's Buildings, West Mains Road, Edinburgh EH9 3JW, UK.

Correspondence to: Jens Zinke, jens.zinke@gmail.com

Abstract

The western Indian Ocean has been warming rapidly over recent decades causing a greater number of extreme climatic events. It is therefore of paramount importance to improve our understanding of links between Indian Ocean sea surface temperature (SST) variability, climate change, and sustainability of tropical coral reef ecosystems. Here we present monthly-resolved coral Sr/Ca records from two different locations from Rodrigues Island (63°E, 19°S) in the south-central Indian Ocean trade wind belt. We reconstruct SST based on a linear relationship with the Sr/Ca proxy with records starting from 1781 and 1945, respectively. We assess relationships between the observed long-term SST and climate fluctuations related to the El Nino-Southern Oscillation (ENSO), the Subtropical Indian Ocean Dipole Mode (SIOD) and the Pacific Decadal Oscillation (PDO) between 1945 and 2006, respectively. The reproducibility of the Sr/Ca records are assessed as are the potential impacts of diagenesis and corallite orientation on Sr/Ca-SST reconstructions. We calibrate individual robust Sr/Ca records with *in-situ* SST and various gridded SST products. The results show that the SST record from Cabri provides the first Indian Ocean coral proxy time series that records the SST signature of the PDO in the south-central Indian Ocean since 1945. We suggest that additional records from Rodrigues Island can provide excellent records of SST variations in the southern Indian Ocean trade wind belt to unravel teleconnections with the SIOD/ENSO/PDO on longer time scales.

1 Introduction

The Indian Ocean has been warming steadily over the past century with the western portion of the basin having experienced an increase in SST of up to 1.2°C over the past 60 years (Koll Roxy et al., 2014). The Indian Ocean has also taken up a large amount of heat in its interior between 1999 and 2016 when global SST increased at a smaller rate compared to previous decades (Lee et al., 2015). The strong Indian Ocean warming over the past century is thought to have contributed to a decreasing land-sea thermal contrast with the Indian subcontinent affecting monsoon rainfall and potentially playing a major role in the decrease in East African rainfall between March to May in recent decades (Funk et al., 2008; Koll Roxy et al., 2015). The western Indian Ocean warming has also been shown to follow closely anthropogenic radiative forcing over the past century (Funk et al., 2008; Alory et al., 2009; Koll Roxy et al., 2015). Furthermore, the western Indian Ocean warmed significantly during past El Niño events with the 1997/98 event causing widespread coral bleaching and mortality (Sheppard, 2003). Synchronously, intrinsic climate modes to the Indian Ocean, like the Subtropical Indian Ocean Dipole Mode during austral summer (SIOD; Fig. 1a; Behera and Yamagata, 2001; Reason, 2001), can interfere with the Indian Ocean-wide teleconnections in SST and rainfall caused by the El Niño-Southern Oscillation (ENSO) or behave independently (Hoell et al., 2016). Mounting evidence indicates that the Pacific Decadal Oscillation (PDO) or Pacific Decadal Variability (PDV) has teleconnections extending to the western Indian Ocean (Fig. 1b; Cole et al., 2000; Crüger et al., 2009). The positive PDO phase corresponds to warm western Indian Ocean SST anomalies (Fig. 1b; Deser et al., 2004), thought to exceed SST anomalies associated with ENSO (Krishnan and Sugi, 2003), particularly in

72 the southwestern Indian Ocean (Meehl and Hu, 2006). It is therefore of paramount
73 importance to improve our understanding of links between Indian Ocean SST variability,
74 global climate change, and sustainability of tropical coral reef ecosystems. Yet, long-term
75 observational records of Indian Ocean SST are sparse and are thought to be only reliable
76 after the 1960's (Tokinaga et al., 2012).

77 Paleoclimate reconstructions of SST from massive corals have provided
78 invaluable records for past SST trends and interannual to decadal variability in the
79 western Indian Ocean (Charles et al., 1997; Cole et al., 2000; Cobb et al., 2001; Pfeiffer
80 et al., 2004, 2009; Pfeiffer & Dullo, 2006; Nakamura et al., 2009; Crueger et al., 2009;
81 Grove et al., 2013a, b; Zinke et al. 2008, 2009, 2014). Massive corals, such as *Porites*
82 spp., can grow for centuries at a rate of 0.5 and 2 $cm.yr^{-1}$. Therefore, down-core
83 geochemical sampling of massive corals can yield reconstructed SST time series at
84 approximately monthly resolution. As the coral precipitates its skeleton, trace elements
85 and stable isotopes are incorporated in proportion to ambient SSTs (Felis and Pätzold,
86 2003). Both, the Sr/Ca ratio and $\delta^{18}O$ composition of the coral aragonite have been shown
87 to be reliable paleo-thermometers with a negative relationship with SST (Alibert and
88 McCulloch, 1997; Pfeiffer & Dullo, 2006; DeLong et al., 2012). A compilation of Sr/Ca-
89 SST calibrations for Porites *spp.* revealed a mean Sr/Ca relationship with SST of -
90 0.061mmol/mol/1°C SST increase (Corrège, 2006). Since Sr has a long oceanic residence
91 time, skeletal Sr/Ca is assumed to mainly reflect SST variability. The quality and
92 accuracy of coral paleo-thermometers strongly depends on optimal sampling of the major
93 growth axes (De Long et al., 2012). Furthermore, diagenetic alteration of coral aragonite
94 can lead to errors in SST reconstructions and it is important that this effect is identified

95 and excluded based on petrographic analysis (McGregor and Gagan, 2003; Hendy et al.,
96 2007; McGregor and Abram, 2008; Sayani et al., 2011; Smodej et al., 2015).

97 Currently, none of the coral proxy records from the western Indian Ocean cover
98 the south-central Indian Ocean basin in the heart of the trade wind system and the
99 Subtropical Indian Ocean Dipole Mode (Fig. 1c). Furthermore, all proxy records of
100 interest for the trade wind belt are based on oxygen isotopes with the exception of two
101 Sr/Ca ratio records covering 1963 to 2008 from St. Marie Island off East Madagascar
102 (Grove et al., 2013a). The latter provided mixed results with discrepancies in terms of the
103 long-term SST trend estimates due to the confounding effects of coral calcification in at
104 least one core (Grove et al., 2013a). A coral oxygen isotope record from Reunion Island
105 (21°S, 55°E; Mascarene Islands) located approximately 230km to the southwest of
106 Mauritius spans the period 1832 to 1994 and is the longest for the subtropical region off
107 East Madagascar (Pfeiffer et al., 2004). Pfeiffer et al. (2004) showed evidence that the La
108 Reunion coral dominantly recorded past variation in salinity associated with transport
109 changes of the South Equatorial Current. The proxy time series records decadal
110 anomalies that were opposite to those of SST. Crüger et al. (2009) reported close linkages
111 of the salinity, sea-level pressure (SLP) and SST signal associated with the Pacific
112 Decadal Oscillation (Mantua et al., 1997) in coral records from Reunion and Ifaty (SW
113 Madagascar), respectively. Two coral oxygen isotope records from the Seychelles located
114 in the tropical western Indian Ocean (5°S, 54°E) were interpreted as an excellent record
115 of past Southwest Monsoon SST changes and showed significant correlations with air
116 temperatures over India between 1847 to 1994 (Charles et al., 1997; Pfeiffer & Dullo,
117 2006). Both, the Reunion and Seychelles records record strong correlations with the

ENSO on interannual and decadal time scales (Pfeiffer & Dullo, 2006). Although the PDO also has a strong impact on the SST in the southwest Indian Ocean (Fig. 1c; Krishnan and Sugi, 2003; Deser et al., 2004), the SST signature of the PDO has not been reported in coral records from this region to date.

Here, we aim to reconstruct past SSTs from Sr/Ca ratios in two coral cores obtained from Rodrigues Island (19°S, 63°E) located 690 km to the North-East of Mauritius within the trade wind belt of the south-central Indian Ocean. To obtain a robust SST record, we assess the reproducibility of the Sr/Ca proxy, and provide a rigorous assessment of the potential impacts of diagenesis and corallite orientation on Sr/Ca-SST reconstructions. We calibrate individual Sr/Ca records with *in-situ* SST and various gridded SST products and verify the suitability of SST products for climate studies in the south-central Indian Ocean. Furthermore, we assess relationships between the observed long-term SST and climate fluctuations related to the ENSO (Kaplan et al., 1998), the SIOD (Behera and Yamagata, 2001) and the PDO (Mantua et al., 1997) between 1945 and 2006, respectively.

2 Regional setting and climate

Rodrigues (63°E, 19°S) is a small volcanic island in the southern Indian Ocean, about 619 km east of Mauritius (Fig. 1c). It is part of the eastern edge of the Mascarene Plateau that comprises Lower Tertiary basalts (Mart 1988) formed by a seaward flow of lava, which has been eroded by hydrodynamic forces, and biological and chemical processes (Turner and Klaus, 2005). Rodrigues has a surface area of about 119 km^2, with a maximum altitude of 396 meter above sea level and is surrounded by a nearly continuous

141 fringing reef approximately 90 km in length (Turner and Klaus, 2005; Lynch et al. 2002).
142 The reef encloses a shallow lagoon, which, at 240km^2, is twice the area of the island
143 itself. The maximum tidal range is approximately 1.5m, and since the average water
144 depth in the lagoon is less than 2m, some areas are exposed at low spring tides. The water
145 depth immediately beyond the reef slopes is usually within the range of 10m to 30m. The
146 island has three major channels, one dredged for the main harbour at Port Mathurin in the
147 north, and natural channels in the south near Port Sud Est and in the East at St Francois.
148 Several small passes are also found around the reef (Turner and Klaus, 2005).
149 The water surrounding Rodrigues is supplied by the South Equatorial Current (SEC)
150 (New et al., 2005, 2007), a broad east to west current between 10º and 20º S in the Indian
151 Ocean driven by the southeast trade winds (Schott and McCreary, 2001). The southern
152 part of the SEC water flows in several directions past Rodrigues occurring mostly in
153 southwest and southeast direction, and westward to Mauritius (New et al., 2005, 2007).
154 Rodrigues has a relatively dry climate and annual mean evaporation exceeds
155 precipitation. Yearly precipitation is ~1000 mm mostly from January to April related to
156 the position of the Inter Tropical Convergent Zone (ITCZ). Between November and
157 March, the Southern Indian Ocean is affected by tropical cyclones, as a result of warm
158 SSTs and a strong convergence between northeast and southeast trades. Rodrigues
159 experiences two to sixteen cyclones per year, of which 2.5 are extreme (category 3 and
160 higher) with winds of 280 km/h and storm surges that reach 100 m inland and 2 m above
161 sea level. They usually last five to ten days (Turner and Klaus, 2005).
162 SST was monitored hourly *in situ* by a conductivity, temperature and depth (CTD)
163 device 150m offshore from the northern fringing reefs at Totor between 2002 to 2006

(Hardman et al., 2004, 2008). Maximum SST are recorded between December to March (28.6 ± 0.5ºC) and minimum SST between July to September (22.4 ± 0.27ºC). Annual mean SST is 25.49 ± 0.24ºC with a seasonal amplitude of 6.22 ± 0.68ºC.

Air temperatures have been recorded by the WMO weather station 61988 (name: Rodrigues, Mauritius) located at the northern coast of Rodrigues since 1951 and are available at http://climexp.knmi.nl/. The most recent years between 1997 and 2007 have been provided by the Rodrigues Meteorological Office. The warmest months are December to March (31.2 ± 0.3º), the coldest months are July to September (24.2 ± 0.3º). Yearly average air temperature is 27.49ºC ± 0.31ºC with a yearly amplitude of about 7 ± 0.79ºC.

3 Materials and Methods

Two coral cores were drilled from massive, dome-shaped *Porites* sp. and *Porites lobata* at the northern reef sites Totor and Cabri, respectively (Fig. 1a; Table 1). The size of the coral colony at Totor is ~2.5m and that of Cabri is ~4m in height. Both colonies were healthy and showed no signs of disease or dead surfaces at the time of drilling. The 220cm long Totor core was obtained in August 2005 from a colony on the forereef slope of the northern fringing reef facing the open ocean with the top of the colony at 4m water depth. The 180cm long Cabri core was obtained in March 2007 from a colony growing in 3m water depth about 1km to the northeast of Totor from the outer fringing reef at Passe Cabri. The site Cabri is more exposed to trade winds as compared to Totor that is more sheltered (Hardman et al., 2004, 2008).

186 A commercially available pneumatic drill driven by scuba tanks was used to
187 extract cores along the central growth axis, with a diameter measuring 4 cm. Cores were
188 sectioned into 7 mm thick slabs, rinsed several times with demineralised water, cleaned
189 with compressed air to remove any surficial particles and dried for more than 24 hours in
190 a laminar flow hood. Annual density bands were visualised by X-radiograph-positive
191 prints, and the growth axis of the coral slab was defined as the line normal to these
192 laminae (Figs. A1 and A2). Coral density (g/cm^3) was calculated by analysing digital X-
193 rays using the program CoralXDS and densitometry (Fig. S1; Helmle et al., 2011;
194 Carricart-Ganivet et al., 2007), calcification rate ($g/cm^2\ yr^{-1}$) by multiplying density with
195 extension rate. The annual extension rates ($cm\ yr^{-1}$) were calculated by measuring the
196 distance (cm) between density minima using the program CoralXDS (Fig. S1). With a
197 diamond coated drill mounted on top of a movable support frame, samples for
198 geochemical analysis were taken every 1 mm parallel to the growth axis, equivalent to
199 approximately monthly resolution.
200 A combination of X-ray images, X-ray diffraction (XRD), light and scanning
201 electron microscopy (SEM) with Energy Dispersive X-Ray Spectrometer (EDS) was used
202 to investigate possible diagenetic alteration in the Totor and Cabri core sections. All core
203 sections from both Totor and Cabri were initially screened for diagenetic alterations using
204 X-ray images (Appendix Figs. 1 and 2). Core sections that showed an annual density
205 banding without anomalous high or low density patches were selected for further study
206 and considered free from obvious diagenetic alteration. Representative samples were
207 selected from both cores based on the X-ray images for SEM, thin-section and XRD
208 analysis. Additional samples were selected along the geochemical sampling tracks

targeting intervals with unusually high or low Sr/Ca ratios. The powder-XRD diffractometer at Rheinisch-Westfaelische Technische Hochschule (RWTH) Aachen University was calibrated to detect and quantify very low calcite contents above ~ 0.2% following the method of Smodej et al. (2015). In addition, the 2D-XRD system Bruker D8 ADVANCE GADDS was used for XRD point-measurements directly on the coral slab with a spatial resolution of ~ 4 mm and a calcite detection limit of ~ 0.2% (Smodej et al., 2015). A 2-dimensional detector allows the simultaneous data collection over a large 2 θ range, which reduces the counting time to 10 min for each sampling spot. The coral is mounted on a motorized XYZ-stage and the position of each sample spot is controlled by an automated laser-video alignment system. Multiple sample points can be predefined and measured automatically. This method was used to test for the presence of secondary calcite along the sampling traces of both corals.

Sr/Ca ratios were measured at the University of Kiel with a simultaneous inductively coupled plasma optical emission spectrometer (ICP-OES, Spectro Ciros CCD SOP; Zinke et al., 2014). Approximately 0.5mg of coral powder was dissolved in 1.00 ml 0.2M HNO_3. Prior to analysis, the solution was diluted with 0.2M HNO_3 to a final concentration of ~8ppm Ca. An analogue in-house coral powder standard (Mayotte) was analyzed after every six samples. The international reference material JCp-1 (coral powder) was analyzed with every sample batch. All calibration solutions are matrix-matched to 8 ppm Ca. Strontium and Ca are measured at their 407 and 317 nm emission lines. Our intensity ratio calibration strategy combines the techniques described by de Villiers et al. (2002) and Schrag (1999). Analytical precision of Sr/Ca

231 determinations as estimated from replicate measurements of unknown samples is 0.15%
232 or 0.01 mmol/mol (1sigma).

233 The coral core chronologies were developed based on the seasonal cycle of Sr/Ca.
234 We assigned the coldest month (either August or September) to the highest measured
235 Sr/Ca ratio (Sr/Ca maxima) in any given year, according to both *in situ* SST and grid-SST
236 (Extended reconstructed SST; Smith et al., 2008). We then interpolated linearly between
237 these anchor points to obtain age assignments for all other Sr/Ca measurements. In a
238 second step, the Sr/Ca data were interpolated to 12 equidistant points per year to obtain
239 monthly time series using AnalySeries 2.0 (Paillard et al., 1996). This approach creates a
240 non-cumulative time scale error of 1 - 2 month in any given year, due to interannual
241 differences in the exact timing of peak SST. The monthly interpolated Sr/Ca time series
242 were cross-checked with the chronologies from coral XDS to reveal the timing of high
243 and low density banding. High density bands in both corals formed in summer (low
244 Sr/Ca) of any given year.

245 We extracted coral proxy data for comparison to our Rodrigues time series from
246 the NOAA paleoclimate data archive (https://www.ncdc.noaa.gov/data-
247 access/paleoclimatology-data/datasets/coral-sclerosponge). We used the time series for
248 the Seychelles (Pfeiffer and Dullo, 2006), La Reunion (Pfeiffer et al., 2004) and St. Marie
249 Island (Grove et al., 2013).

250

251 **4 Historical SST data and climate indices**

252 Historical SST data collected primarily by ships-of-opportunity have been summarised
253 in the comprehensive ocean atmosphere data set (ICOADS) to produce monthly averages

254 on a 2x2° grid basis (Woodruff et al., 2005). In the grid that includes Rodrigues Island
255 the data are extremely sparse (Fig. A3). Since the uncertainty in SST bias adjustments
256 due to measurement errors is much larger for Southern Hemisphere than the Northern
257 Hemisphere (Jones, 2016) data, we therefore extracted various SST and marine air
258 temperature datasets for our region for comaprison with our coral proxy data. We
259 extracted SST from extended reconstructed SST (ERSST version 3b/version 4; Smith et
260 al., 2008), also based on ICOADS data, which uses sophisticated statistical methods to
261 reconstruct SST from sparse data. From ERSST, we extracted data in the 2x2° grid
262 centred at 61-63°E, 19-21°S (Table A1). Furthermore, we used Met Office Hadley
263 Centre's sea ice and sea surface temperature (HadISST) data for the grid 62-63°E, 19-
264 20°S (Rayner et al., 2003; Kennedy et al., 2011). HadISST temperatures were
265 reconstructed using a two-stage reduced-space optimal interpolation procedure, followed
266 by superposition of quality-improved gridded observations onto the reconstructions to
267 restore local detail. Since January 1982, SST time series for HadISST use the optimal
268 interpolation SST (OISST; 1x1°), version 2 (Reynolds et al., 2002) that includes
269 continuous time series of satellite-based SST measurements. We also extracted Advanced
270 Very High Resolution Radiometer (AVHRR) SST at 0.25x0.25° resolution (Reynolds et
271 al., 2007; Tab. A1) from 1985 to 2006 . SST from the 5x5° HadSST3, the most
272 sophisticated bias-corrected SST data to date, were downloaded for the region 60-65°E,
273 15-20°S (Kennedy et al., 2011) but contains data gaps throughout the record due to strict
274 quality control. SST is reported as anomalies relative to the 1961 to 1990 mean
275 climatology. In addition, we extracted 5x5° nigh-time marine air temperature data from
276 HadMAT1 and HadNMAT2 datasets (Kent et al., 2013). HadNMAT2 also contains data

277 gaps throughout the record due to strict quality control. Night-time marine surface air
278 temperature is highly correlated with SST but free of the biases introduced by changes in
279 SST measurement techniques (Tokinaga et al., 2012).
280 All climate indices used for comparison with instrumental and coral proxy data were
281 extracted from the Royal Netherlands Meteorological Institute (KNMI) online tool
282 climate explorer (Trouet and Oldenborgh, 2005). We extracted the time series for the
283 Subtropical Indian Ocean Dipole Mode (SIOD; Behera and Yamagata, 2001), the El
284 Niño-Southern Oscillation (ENSO; Kaplan et al., 1998) and the Pacific Decadal
285 Oscillation (PDO; Mantua et al., 1997).
286 Statistical analysis includes linear correlation for linearly detrended data only with
287 climate indices and instrumental data with 95% confidence limits indicated for the
288 correlation coefficients using a Monte Carlo approach (Trouet and Oldenborgh, 2005; see
289 Supplementary Data). Spatial correlations for linearly detrended data only were computed
290 at knmi climate explorer (van Oldenborgh and Burgers, 2005) taking into account only
291 correlations with $p<0.05$.
292

293 **5 Results**

294 **5.1 Coral Sr/Ca seasonality, variability and trends**

295 The average growth rate of the corals Totor (224 years) and Cabri (130 years)
296 were 9.82±0.19mm y^{-1} and 11.79±0.25mm y^{-1}, respectively (Table 1; Fig. S1). The Cabri
297 core shows a growth disturbance at 1907 that led to partial colony mortality (see Suppl.
298 Information). This lower core section is overprinted by diagenesis and it is therefore not
299 suitable for climate studies or to determine density and calcification rates.

For the period of overlap (1945 to 2005) there is an offset in mean Sr/Ca of 0.0242 mmol/mol between the two colonies. Both cores show a distinct seasonality in Sr/Ca throughout their record length. The seasonality in the Totor core (0.283±0.049 mmol/mol) is on average slightly higher compared to the Cabri core (0.238±0.055 mmol/mol), yet the difference is not statistically significant (both overlap within 1σ). To eliminate the offset between Sr/Ca time series we calculated Sr/Ca anomalies by subtracting their mean relative to the 1961 to 1990 reference period (Fig. 2a).

Between 1945 and 2006 both cores record higher Sr/Ca anomalies relative to 1961-1990 (a period of cooling) that started in the mid 1950's and lasted until the early 1970's. Both cores show a pronounced trend to more negative Sr/Ca values (warming) starting in the 1970's (Fig. 2a). After 1984 Sr/Ca in the Cabri core further decreases (warms) while Sr/Ca in the Totor core records no trend. This highlights that the long-term trend estimates after 1984 need to be viewed with caution.

The Sr/Ca time series in the Totor core extends to 1781 (Fig. 2a). Marked negative Sr/Ca anomalies (warmer) are observed during the first half of the 20th century centered at 1918/19, 1936-41 and in the period 1948-1951 that exceed anomalies in the 1961 to 1990 reference period. Sr/Ca anomalies between 1850 and 1890 are higher (cooler) while decadal periods with lower (warmer) Sr/Ca are observed between 1781 and 1850 relative to 1961 to 1990.

5.2 Diagenetic tests for alterations of Sr/Ca profiles

Representative samples for diagenetic screening with XRD, SEM and light microscopy were identified on the coral slabs using the X-radiographs (Fig. A1 and A2).

Additionally, intervals with presumably anomalous proxy values (warm or cold anomalies) were analyzed with the same methods. Ten thin-sections, six SEM samples, ten powder-XRD and thirteen spot-2D-XRD samples were analyzed from coral core Totor (Fig. 3). For coral core Cabri, seven thin-sections, one powder-XRD and six 2D-XRD samples were analyzed. Neither powder nor spot-XRD analysis detected any calcite. Thin-section analysis indicates a growth break within core section 12 of Totor that is also apparent in the radiograph (Fig. A1). Close to this break the coral is strongly affected by bioerosion and encrustation by red algae (Fig. 3e). The sampling transect for geochemical analysis, however, excluded this area and therefore the reported data are not affected by diagenesis. Combined SEM, EDS and XRD analysis shows low amounts of patchy distributed isopachous (~2μm) fibrous aragonite cement in Totor core section 6 (1916-1921), 7 (1882-1887) and 11 (~ 1809).

Aragonite cement should lead to higher Sr/Ca values and lower reconstructed temperatures (Hendy et al., 2007). An interesting outcome is that the observed diagenesis is not able to explain changes in the Sr/Ca ratios except for the Totor core section 7. Here the observed aragonite cement is associated with relatively high Sr/Ca values resulting in an apparent cold anomaly. No anomalously high Sr/Ca ratios are associated with the patchy aragonite cements in Totor core sections 6 and 11. Instead core sections 6 and 11 are characterized by low Sr/Ca ratios resulting in apparent relatively warm reconstructed temperatures. All other samples from the core sections Totor 3, 4, 8, 9 and 10 are devoid of diagenetic alteration. In summary, a diagenetic influence on the proxy record and resulting SST reconstructions are only evident for Totor core section 7 (years 1882-1887). Core Cabri showed only localized (single month) positive Sr/Ca anomalies (cool

346 SST bias; Fig. 3f). Thin-section and XRD analysis did not establish any diagenetic
347 alteration, but the coral locally contained aragonitic sediment partially filling pore spaces
348 (Fig. 3f). This aragonitic sediment potentially could have caused the isolated Sr/Ca peaks
349 (high Sr/Ca) in the record. These individual data points were omitted from further
350 analysis.
351
352 **5.3. Calibration of coral Sr/Ca-SST with in-situ and gridded SST**
353 SST seasonality does not differ significantly between SST products for the 2002
354 to 2006 period for which we had *in situ* SST. Therefore, the coral Sr/Ca from both cores
355 was calibrated with *in situ* SST, ERSSTv.3b and AVHRR SST for the period 2002 to
356 2006 using the minima and maxima in any given year, as well as monthly values with
357 AVHRR SST for 1981 to 2006 (Fig. 4; Tab. A2). There is a relatively large variance in
358 the Sr/Ca-SST relationships depending on the coral core and the SST record. The slopes
359 of the ordinary least squares regressions vary between -0.0384 to -0.0638 mmol/mol per
360 1°C (Tab. A2). The lowest slopes are obtained with *in situ* SST and the highest with
361 ERSSTv.3b (Tab. A2). The range of this variance is consistent with the results of Corrège
362 (2006), who used a set of more than 30 coral Sr/Ca records from various ocean basins and
363 different coral genera. We reconstructed absolute SST for the period of overlap with *in*
364 *situ* SST from 2002 to 2006 from both coral cores (Fig. 4). The Sr/Ca-SST in the Totor
365 core shows the best fit with *in situ* SST in terms of the seasonal amplitude. The Sr/Ca-
366 SST in the Cabri core overestimates the winter SST of 2002 and 2005, yet agrees well for
367 2003 and 2004 (Fig. 4). Taking into account the uncertainties (measurement error,

368 regression error) in absolute SST from Sr/Ca for Cabri and Totor of 1.23°C and 1.05°C
369 (1σ), respectively, the coral data agree with *in situ* SST within the 1σ uncertainty.
370
371 **5.4. Validation of Sr/Ca-SST anomalies with gridded SST products**
372 To eliminate errors associated with absolute SST reconstructions from coral Sr/Ca
373 we calculated relative changes in SST for the coral temperature records relative to the
374 1961 to 1990 mean based on the established empirical relationship of -0.0607 mmol/mol
375 per 1°C derived from >30 published Sr/Ca calibrations (Corrège, 2006; Nurhati et al.,
376 2011). This slope is well within the range of our regressions based on a variety of SST
377 datasets and consistent with the results of Corrège (2006). (Tab. A2). We consider the
378 mean Sr/Ca-SST slope of Corrège (2006) to be much more reliable than our short *in situ*
379 calibration. We use a conservative estimate of the uncertainty around relative SST
380 changes based on the difference between lower (-0.04) and upper slope (-0.084) estimates
381 from these regression equations, thus ± 0.02 mmol per 1°C or ±0.33°C (following Gagan
382 et al., 2012; Tab. A2).
383 We validated the coral derived annual mean SST reconstruction against local Air
384 Temperature (AT), ERSSTv3b, ERSST4, HadISST, HadSST3, HadMAT1 and
385 HadNMAT2 for the period 1951 to 2006 (Fig. 5; See Supplementary Tables 1-16 for
386 mean annual correlations). We stress that the number of SST observations in the
387 ICOADS SST and marine AT database is extremely sparse for our region (Fig. A3). The
388 Cabri coral SST record records the highest correlations with HadISST and HadMAT1 in
389 the grid box surrounding Rodrigues Island (Fig. A4) while the overall best fit is obtained
390 with local Rodrigues AT. Core Totor has no significant correlations with both ERSST

391 products and HadISST, yet shows significant correlations with HadSST3, HadMAT1 and
392 HadNMAT2 (; Suppl. Tabs. 11, 15, 16). Discrepancies between AT and gridded SST
393 products are observed between 1951 and 1955 with AT indicating significantly warmer
394 temperatures. Cabri tracks grid-SST between 1951 and 1955 while Totor shows warm
395 anomalies similar to AT. Taking into account the uncertainty of ±0.33°C based on the
396 regression error, however, Cabri SST agrees with gridded SST and AT within 1σ while
397 Totor shows less agreement.

398 For the period 1951 to 2005, we used AT, ERSSTv3b, ERSST4, HadISST,
399 HadSST3, HadMAT1 and HadNMAT2 to validate trends in annual mean coral Sr/Ca-
400 SST anomalies (Fig. 5). The uncertainty for the trend estimates in coral Sr/Ca SST is
401 calculated from the square root of the sum of squares of the regression error and the error
402 in the slope of the Sr/Ca-SST relationship. The long-term trends in Sr/Ca-derived SST
403 anomalies for the period 1951 to 2005 for Cabri and Totor converted to SST, using the
404 published Sr/Ca-SST relationship of -0.0607mmol/mol per 1°C, indicate a warming of
405 1.38±0.39°C and cooling of -0.49±0.41°C, respectively. Instrumental SST indicate a
406 warming trend of 0.61±0.13°C for HadISST, 0.72±0.11°C for ERSST3b (0.86±0.12°C
407 for ERSST4) and 0.78±0.12°C for HadSST3. Air Temperature at Rodrigues weather
408 station recorded a warming trend of 0.46±0.17°C. All trends are statisctically significant
409 at the 98% level with the exception of the negative trend in Sr/Ca SST anomalies in the
410 Totor core which is not significant.

411 For the pre-1945 period we used ERSSTv3b, HadISST, HadSST3 HadMAT1 and
412 HadNMAT2 to validate annual mean coral Sr/Ca-SST from core Totor (Fig. 2). We stress
413 that the number of SST observations in the ICOADS SST and marine AT database is

414 extremely sparse for our region (Fig. A3). In general, the Totor SST record is a valid
415 reconstruction for the region surrounding Rodrigues Island for several decades with the
416 possible exception of 1854-1860, 1916-1921, 1936-1941 and 1948-1951 (Fig. 2). The
417 Totor coral SST time series displays significantly higher SST anomalies compared to all
418 gridded SST reconstructions in the 1850's, between 1916-1921, 1936-1941 and 1948-
419 1951 and lower SST anomalies for brief periods between 1850 and 1890. Interestingly,
420 the Totor Sr/Ca-SST has significant correlations with HadSST3, HadMAT1 and
421 HadNMAT2 observational time series only (Suppl. Tabs. 11, 15, 16). The cool bias in
422 coral derived SST between 1882 and 1887 (core section 7) is related to diagenetic
423 alterations, but none of the anomalously warm periods can be explained by diagenesis
424 (see next section). We assessed the orientation of corallites relative to the coral slab
425 surface to test for sampling artifacts that might have altered our Sr/Ca data which we
426 summarized in Tables 2 and 3, illustrate in Figure 2 and discuss in section 6.1. Most
427 anomalous warm periods show sub-optimal orientation of sampling path with corallites at
428 an angle to the slab surface (see 6.1).
429
430 **5.5 Large scale teleconnections between 1945 and 2006**
431 The large-scale teleconnections with SST are significant for the Cabri Sr/Ca-SST
432 time series starting in 1945 (Figs. 6 and 7), while core Totor has statistically insignificant
433 correlations in that period. This indicates that the Cabri time series is more reliable for the
434 recent 60 years for monthly averages and annual means and shows the strongest
435 correlations across the Indo-Pacific (Figs. 6 and 7). Therefore, we assess the large-scale
436 climate teleconnections only for the period between 1945 and 2006.

437 The detrended Cabri Sr/Ca-SST records shows significant positive correlations for
438 austral summer and annual means with Indian Ocean wide SST, a positive significant
439 correlation with the central and eastern Pacific SST and negative significant correlations
440 with North Pacific SST typical for the spatial ENSO and PDO pattern (Figure 6;
441 Supplementary Tables 17-19). The detrended mean annual time scales (July-June) and
442 austral summer (JFM) record for the Cabri SST indicates a positive significant correlation
443 with southern Indian Ocean SST along a southeast to northwest band stretching along the
444 trade wind belt (Figure 6d-f). The correlation with the southern Indian Ocean trade wind
445 belt remains stable over different record length and is most pronounced post 1971. The
446 detrended Cabri record shows negative significant correlations ($r= -0.39$; $p<0.001$; $N=48$)
447 with the SIOD index for austral summer month. This agrees with similar sign and
448 strength of correlations of HadISST for Rodrigues with the SIOD ($r= -0.43$; $p<0.001$;
449 $N=48$; Fig. 1a; Tab. S19-21). We find positive significant correlations with the eastern
450 Pacific SST and negative correlations with the northern Pacific along 40°N and stretching
451 between 160°E and 150°W. The SST pattern mimics part of the typical spatial ENSO and
452 PDO pattern across the Indo-Pacific (Mantua et al., 1997; McPhaden et al., 2006).
453 Stratifying the correlations into negative and positive PDO phases between 1950-1975
454 and 1976 to 1999 reveals the PDO-like spatial SST pattern (Fig. 7).
455 Comparison with available coral proxy records from the wider trade wind belt
456 region in the SWIO between 12 to 21°S and 50 to 63°E reveals that the Cabri record
457 agrees best with the Sr/Ca-SST from St. Marie Island (core STM2 in Grove et al., 2013a;
458 $r=0.25$; $N=50$, $p=0.08$; Fig. 8) on mean annual time scales, yet not with the La Reunion
459 record (not shown). Cabri shows the highest significant correlation of the three coral

460 records from SWIO with HadISST for the larger grid-box between 12 to 21°S and 50 to
461 63°E (r=0.49, p=0.001, N=60) while both St. Marie and La Reunion corals show no
462 statistically significant correlations.
463
464 **6 Discussion**
465 **6.1 Diagenesis, coral growth pattern changes and potential biases in Sr/Ca derived**
466 **SST**
467 Generally diagenesis could be excluded as a major cause of discrepancies between
468 coral SST and grid-SST. For core Totor, only for the period between 1882 and 1887 is
469 diagenesis the cause of a cool bias on our coral SST reconstruction (Figure 3d). Core
470 Cabri showed only localized positive Sr/Ca anomalies (cool SST bias) caused by
471 aragonitic sediment trapped within growth framework pores (Fig. 3f). These specific
472 samples have been removed before interpolation. Having excluded diagenesis for almost
473 all of the record, we assessed sampling biases due to changes in the orientation of growth
474 axes and positioning of corallites to the slab surface (Tab. 2 and 3). De Long et al. (2012)
475 showed clear evidence for warm or cool biases in coral Sr/Ca-SST reconstructions caused
476 by suboptimal orientation of corallites in corals from New Caledonia. We have adopted a
477 similar approach to test for sampling biases in our two cores (summarized in Table 2 and
478 3). We found that core Totor contained areas where a sampling bias could explain
479 anomalous Sr/Ca-derived SST (1781-1797, 1825-1835, 1854-1860, 1916-1921, 1936-
480 1941 and 1948-1951, 1984-2001). We provide a detailed explanation of the potential
481 biases in core Totor and its co-variability with a tropical western Indian Ocean coral SST

482 reconstruction from the Seychelles pre-1900 (Pfeiffer and Dullo, 2006; Fig. S2) in the
483 Supplementary Information that is of particular importance for coral paleoclimatologists.
484 De Long et al. (2012) showed that warm biases were often caused by corallites
485 orientated at an angle to the slab surface and where growth orientation had changed.
486 Sampling of these suboptimal intervals will have seasonal cycles with more summer
487 Sr/Ca values than winter values causing an apparent warm bias. Such a relationship could
488 not be identified for core Totor, for instance for the largest single warm anomaly in the
489 years 1916 to 1921. Nevertheless, the extreme warm anomaly between 1916 to 1921
490 could be associated with an unidentified vital effect (Alpert et al., 2015). Interestingly,
491 despite the potential influence of vital effects on the trend, the seasonality in this core
492 section was well preserved. This implies that seasonality can be captured robustly while
493 absolute values and trends are potentially biased by vital effects. This adds confidence for
494 the study of seasonality from fossil corals where vital effects are harder to distinguish
495 from true variability due to the lack of SST data for verification.
496 For the core tops between 1984 and 2005, Sr/Ca trends in cores Totor and Cabri
497 deviate with Totor showing a statistically insignificant cooling trend while Cabri shows a
498 strong warming trend (Fig. 2). Our analysis of polyp growth revealed a change in growth
499 pattern near the top of core Totor: the corallites form parallel, elongated rods of septa for
500 the entire period 1984 to 2005 (Fig. 9). Cabri shows a normal growth pattern, with an
501 optimal orientation of corallites at the core top between 1984 and 2006 (Fig. A5), with
502 the exception of sub-optimal corallites in the period 2000 to 2006. The core top of the
503 Totor coral skeleton has very low overall density compared to the pre-1984 record. The
504 Sr/Ca ratios show an increased seasonality, with colder winter values compared to core

505 Cabri, while summer values are not affected. At first glance, the peculiar structure of the
506 corallites in Totor would suggest optimal vertical growth of the corallites with the polyps
507 clearly visible from the apex of the core slab. This structure is, however, clearly
508 associated with high Sr/Ca ratios and artificially cold SST anomalies. A similar growth
509 pattern was found in a *Porites lutea* from St. Marie Island off East Madagascar (core
510 STM4 in Grove et al. 2013a). Grove et al. (2013a) ascribed the Sr/Ca trend difference
511 between cores STM2 and STM4 to changes in coral growth and calcification, yet their
512 results were not conclusive. Re-examination of core STM4 revealed that it also forms the
513 parallel-elongated rods of septa in the core top, which was biased towards high Sr/Ca
514 ratios and therefore cold SST anomalies. STM4 also showed low densities in this core top
515 section that agrees with low density in Totor. Inspection of various core sections in Totor
516 and other coral cores revealed that similar elongated rods of septa (not sampled down
517 core) are formed between neighboring growth fans of septa. We propose that these
518 parallel septa grow very fast in summer and winter, therefore show weak density contrast
519 with overall low skeletal density. Similar anomalously high Sr/Ca values between
520 adjacent fans of corallites were reported for Great Barrier Reef corals (see Figure 4 in
521 Alibert and McCulloch, 1997). Alibert and McCulloch (1997) suggested that less optimal
522 growth conditions may results in smaller corallites and overall low skeletal density
523 affecting Sr/Ca ratios. We suggest that core tops from *Porites* sp. with similar parallel
524 septa should be avoided for sampling since it can cause a cold bias in Sr/Ca-based SST
525 reconstructions.

526 Overall, our test for sampling biases to a large extend confirms the findings of De
527 Long et al. (2012) and indicates that such analysis should accompany climate

528 reconstructions from coral cores. Our results suggest that new cores need to be obtained
529 from the Totor colony or other large *Porites* sp. in order to overcome the SST biases
530 identified in the current record. The Cabri coral (>3.5m in height) would be an ideal site
531 since it provided an excellent and largely un-biased record of SST for the period 1945 to
532 2006. The 1907 dead surface was present, however, in three long cores drilled from the
533 Cabri coral at different angles, which could undermine the SST reconstruction for a few
534 decades below the mortality event. The reason for the mortality event could not be
535 determined.
536
537 **6.2 Trends and large-scale climate teleconnections since 1945 from core Cabri**
538 Based on our analysis of corallite orientations and diagenesis, we conclude that
539 core Cabri provides a largely un-biased record to assess SST trends and interannual
540 variability since 1945. The Cabri time series recorded a higher SST rise (1.38±0.41°C)
541 than instrumental data between 1945 and 2006, which ranged between 0.61 to
542 0.86±0.15°C. The trend in Cabri agrees with all SST datasets within 2σ, whereby the
543 lower range of uncertainty for the Cabri trend estimates (~1°C) is in close agreements to
544 trends from gridded SST datasets. Most of the accelerated warming trend in Cabri
545 resulted from the recent 6 years where the orientation of the corallites was sub-optimal.
546 We conclude that the SST trend in Cabri closely follows open ocean grid-SST which both
547 indicate strong warming (~0.68-1°C) of the south-central Indian Ocean over the past 60
548 years. Roxy et al. (2014) reported that during 1901–2012, the Indian Ocean warm pool
549 warmed by 0.78°C while the western Indian Ocean (5°S–10°N, 50°–65°E) experienced
550 anomalous warming of 1.28°C in summer SSTs. Our results for Cabri are therefore not

551 unusual and within the range of observed Indian Ocean SST trends (Annamalei et al.,
552 2005; Alory et al., 2007; Koll Roxy et al., 2014). The strong warming in the southern
553 Indian Ocean trade wind belt could potentially alter the monsoon circulation, especially
554 during the monsoon onset phase in austral autumn (March to May; Annamalei et al.,
555 2005). Both, our Cabri coral SST time series and SST products indicate the strongest
556 warming for the March to May season (not shown). Rodrigues station precipitation is
557 strongly positively correlated with SST between March and May. When precipitation is
558 anchored over a warmer SWIO between March and May it can prevent the movements of
559 the ITCZ towards the North and potentially disrupt the Asian monsoon onset (Annamalei
560 et al., 2005).

561 The Cabri record also indicated that Rodrigues Island has negative correlations
562 with the SIOD. Rodrigues Island is located at the westernmost edge of the northeastern
563 flank of the SIOD that stretches from the south-central western Indian Ocean to the coast
564 of Western Australia. There is no other coral reef between Rodrigues Island and the West
565 Australian coast that is able to track the SIOD. Rodrigues is therefore the only coral reef
566 at which SST variability tracks the SIOD at its northeastern flank. The Ifaty corals off
567 southwest Madagascar was shown to track the southwestern flank of the SIOD (Zinke et
568 al., 2004). Our results suggest that a combination of corals off southwest Madagascar
569 with longer records from Rodrigues could provide valuable records of past SIOD
570 variability.

571 The Cabri coral SST reconstructions revealed a clear ENSO/PDO teleconnection
572 pattern for mean annual and austral summer averages with positive correlations across the
573 Indian Ocean in response to ENSO and PDO (Xie et al., 2016; Fig. 6 and 7; Suppl. Tabs.

574 17-19). The ENSO/PDO teleconnection was stable for the recent 60 years, yet appears
575 strongest between 1971 and 2006 (Fig. 6c,f). The latter period is known for increased
576 occurrence of El Niño events and a switch to a positive PDO phase up to 1999
577 (McPhaden et al., 2006). These results are in agreement with ENSO/PDO pattern
578 correlations observed in other coral records from the southwestern Indian Ocean (Pfeiffer
579 et al., 2004; Crüger et al., 2009). This is the first Indian Ocean coral SST reconstruction,
580 however, that shows a clear Indian Ocean SST relationship with the PDO. Previous
581 studies have shown only indirect links between the PDO with southwestern Indian Ocean
582 sea level pressure and salinity (Crueger et al., 2009), hydrological balance (Zinke et al.,
583 2008) and river runoff (Grove et al., 2013b). In addition, our record is the first Sr/Ca
584 record for the south-central Indian Ocean, which is currently the most reliable proxy for
585 SST in corals. The only long record from this region of the Indian Ocean is a stable
586 isotope record from La Reunion Island that mainly records salinity variations (Pfeiffer et
587 al., 2004). The lack of correlation between the La Reunion and Cabri record is therefore
588 not surprising and points to the need to develop Sr/Ca time series for La Reunion. The St.
589 Marie Island Sr/Ca coral record shows reasonable agreement with Cabri, with the SST
590 shift in the 1970's especially apparent in both records (Fig. 8). The St. Marie Island
591 record is, however, not well suited to track the wider trade wind belt variations.
592 Therefore, our new proxy record from Rodrigues for the period between 1945 and 2006 is
593 a valuable addition to the sparse Indian Ocean coral proxy network. It also establishes
594 that records from Rodrigues are well suited to study decadal climate teleconnections with
595 the (extra)tropical Pacific and the wider Indian Ocean.
596

7 Acknowledgements

The coral paleoclimate work was supported as part of the SINDOCOM grant under the Dutch NWO program 'Climate Variability', grant 854.00034/035. Additional support comes from the NWO ALW project CLIMATCH, grant 820.01.009, and the Western Indian Ocean Marine Science Association through the Marine Science for Management program under grant MASMA/CC/2010/02. We thank the team of SHOALS Rodrigues for their excellent support in fieldwork logistics and in the organization of the research and CITES permits. We would also like to thank the Rodrigues Assembly and the Mauritius Ministry for Fisheries for granting the research and CITES permits. A Senior Curtin Fellowship in Western Australia, and an Honorary Fellowship with the University of the Witwatersrand, South Africa, supported JZ. Bouke Lacet and Wynanda Koot (VUA) helped cut the core slabs and prepared the thin sections. Janice Lough and Eric Matson (AIMS) provided skilled technical support for coral core densitometry measurements and data processing. We thank Dieter Garbe-Schönberg for assistance with the ICP-OES measurements.

References

Alibert, C. and McCulloch M. T.: Strontium/calcium ratios in modern Porites corals from the Great Barrier Reef as a proxy for sea surface temperature: calibration of the thermometer and monitoring of ENSO, Paleoceanography, 12(3), 345-363, 1997.

Alory, G. and Meyers, G.: Warming of the Upper Equatorial Indian Ocean and Changes in the Heat Budget (1960–99), J. Climate, 22, 93–113, 2009.

Alpert, A. E., Cohen, A. L., Oppo, D. W., DeCarlo, T. M., Gove, J. M., Young, C. W. Comparison of equatorial Pacific sea surface temperature variability and trends with Sr/Ca

623 records from multiple corals. Paleoceanography, 31, 252-262, 2016.

624 Annamalai, H., Liu, P. and Xie, S.-P.: Southwest Indian Ocean SST Variability: Its Local
625 Effect and Remote Influence on Asian Monsoons, Journal of Climate, 18, 4150-4167, 2005.
626 Behera, S.K. and Yamagata, T. Subtropical SST dipole events in the southern Indian
627 Ocean, Geophys. Res. Lett. 28 (2), 327– 330, 2001.
628
629 Behera SK, Yamagata T. A dipole mode in the tropical Indian Ocean. Geophysical Research
630 Letters, 28, 327–330, 2001.
631
632 Carricart-Ganivet, J. P. and Barnes D. J.: Densitometry from digitized images of X-
633 radiographs: methodology for measurement of coral skeletal density, Journal of Experimental
634 Marine Biology and Ecology, 344, 67-72, 2007.
635
636 Charles, C. D., Hunter, D. E. and Fairbanks R. G.: Interaction between the ENSO and the Asian
637 Monsoon in a coral record of tropical climate, Science, 277, 925-928, 1997.
638
639 Cobb, K. M., Charles, C. D. and Hunter D. E.: A central tropical pacific coral demonstrates
640 pacific, Indian, and Atlantic decadal climate connections, Geophysical Research Letters 28(11),
641 2209-2212, 2001.
642
643 Cole, J. E., Dunbar, R. B., McClanahan, T. R. and Muthiga N. A.: Tropical Pacific forcing of
644 decadal SST variability in the Western Indian Ocean over the past two centuries. Science 287,
645 617-619, 2000.
646
647 Corrège, T., Sea surface temperature and salinity reconstruction from coral geochemical
648 tracers. Palaeogeo. Palaeoclim. Palaeoeco., 232, 408-428, 2006.
649
650 Crueger, T., Zinke, J. and Pfeiffer M.: Patterns of Pacific decadal variability recorded by Indian
651 Ocean corals. International Journal of Earth Sciences 98, doi:10.007/s00531-00008-00324-
652 00531, 2009.
653

654 Deser, C., Phillips, A. S., and Hurrell, J. W.: Pacific Interdecadal climate variability:
655 linkages between the tropics and the North Pacific during boreal winter since 1900, J.
656 Climate, 17, 3109-3124, 2004.
657
658 DeLong, K. L., Quinn, T. M., Taylor, F. W., Shen, C.-C. and Lin, K.: Improving coral-base
659 paleoclimate reconstructions by replicating 350 years of coral Sr/Ca variations,
660 Palaeogeography, Palaeoclimatology, Palaeoecology, 373, 6-24, 2012.
661
662 DeVilliers, S., Sheng, G.T., Nelson, B.K.: The Sr /Ca-temperature relationship in coralline
663 aragonite: Influence of variability in (Sr/Ca)seawater and skeletal growth parameters,
664 Geochimica et Cosmochimica Acta, 58, 197-208, 1994.
665
666 Felis, T. and Paetzold, J.: Climate records from corals, In: Marine Science Frontiers for
667 Europe. Eds.: G. Wefer, F. Lamy and F. Mantoura. Berlin, Heidelberg, New York, Tokyo,
668 Spinger, p. 11-27, 2003.
669
670 Funk, C., Dettinger, M. D., Michaelsen, J. C., Verdin, J. P., Brown, M. E., Barlow, M. and
671 Hoell, A.: Warming of the Indian Ocean threatens eastern and southern African food security
672 but could be mitigated by agricultural development, Proceedings Nat. Acad. Sci., 105(32),
673 11081-11086, 2008.
674
675 Gagan, M. K., Dunbar, G. B. and Suzuki, A.: The effect of skeletal mass accumulation in
676 Porites on coral Sr/Ca and d18O paleothermometry, Paleoceanography 27, PA1203,
677 doi:10.1029/2011PA002215, 2012.
678
679
680 Grove, C. A., Kasper, S., Zinke, J., Pfeiffer, M., Garbe-Schönberg, D. and Brummer, G.-J. A.:
681 Confounding effects of coral growth and high SST variability on skeletal Sr/Ca: Implications
682 for coral paleothermometry, Geochem., Geophys. Geosyst., 14, doi:10.1002/ggge.20095,
683 2013a.
684

685 Grove, C. A., Zinke, J., Peeters, F., Park, W., Scheufen, T., Kasper, S.,
686 Randriamanantsoa, B., McCulloch, M. T. and Brummer, G.J.A. Madagascar corals reveal
687 multidecadal modulation of rainfall since 1708. Climate of the Past 9, 641-656, 2013b.
688
689 Hardman, E. R., Meunier, M. S., Turner, J. R., Lynch, T. L., Taylor, M. and Klaus R.: The
690 extent of coral bleaching in Rodrigues, Journal of Natural History, 38, 3077-3089, 2004.
691
692 Hardman, E. R., Stampfli, N. S., Hunt, L., Perrine, S., Perry, A. and Raffin, J. S.: The Impacts
693 of coral bleaching in Rodrigues, Western Indian Ocean, Atoll Research Bulletin, 555, DOI:
694 10.5479/si.00775630.555.1, 2008.
695
696 Helmle, K. P., Dodge, R.E., Swart, P.K., Gledhill, D.K. and Eakin, C.M.: Growth rates of
697 Florida corals from 1937 to 1996 and their response to climate change, Nat. Commun, 2, 215
698 doi: 10.1038/ncomms1222, 2011.
699
700 Hendy, E. J., Gagan, M. K., Lough, J. M., McCulloch, M., and deMenocal P. B.: Impact of
701 skeletal dissolution and secondary aragonite on trace element and isotopic climate proxies in
702 Porites corals, Paleoceanography, 22, PA4101, doi:10.1029/2007PA001462, 2007.
703
704 Hoell, A., Funk, C., Zinke, J., Harrison, L. Modulation of the Southern Africa precipitation
705 response to the El Niño Southern Oscillation by the subtropical Indian Ocean Dipole. Climate
706 Dynamics, DOI:10.1007/s00382-00016-03220-00386, 2016.
707
708 Jones, P. The Reliability of Global and Hemispheric Surface Temperature Records. Advances in
709 Atmospheric Sciences, 33, 269-282, 2016.
710
711 Kaplan, A., Cane, M. A., Kushnir, Y., Clement, A. C., Blumenthal, M. B., Rajagopalan, B.
712 Analyses of global sea surface temperature 1856-1991, J. Geophys. Res., 103, 18567-18589,
713 1998.
714
715 Kennedy J.J., Rayner, N.A., Smith, R.O., Saunby, M. and Parker, D.E.: Reassessing biases and

716 other uncertainties in sea-surface temperature observations since 1850 part 1: measurement and
717 sampling errors, J. Geophys. Res., 116, D14103, doi:10.1029/2010JD015218, 2011.
718
719 Kent, E.C., Rayner N.A., Berry D.I., Saunby M., Moat B.I., Kennedy J.J., Parker D.E.: Global
720 analysis of night marine air temperature and its uncertainty since 1880: the HadNMAT2
721 Dataset, Journal of Geophys. Res., doi: 10.1002/jgrd.50152, 2013.
722
723 Koll Roxy, M., Ritika, K., Terray, P., Masson, S.: The curious case of Indian Ocean warming,
724 Journal of Climate 27, 8501-8509, 2014.
725
726 Krishnan, P., and Sugi, M.: Pacific decadal Oscillation and variability of the Indian
727 summer monsoon rainfall, Climate Dynamics, 21, 233-242, 2003.
728
729 Lee, S.-K., Park, W., Baringer, M. O., Gordon, A. L., Huber, B. and Liu ,Y.: Pacific origin of
730 the abrupt increase in Indian Ocean heat content during the warming hiatus, Nature Geoscience,
731 8, 445-449, 2015.
732
733 Lynch T.L., Meunier, M.S., Hooper, T.E.J., Blais, F.E.I., Raffin, J.S.J, Perrine, S., Félicité, N.,
734 Lisette, J., Grandcourt, J.W.: Annual report of benthos, reef fish and invertebrate surveys for
735 Rodrigues 2002, Shoals Rodrigues report, 30pp, 2002.
736
737 Mantua, N. J., Hare, S. R., Zhang, Y., Wallace, J. M., and Francis, R. C.: A Pacific decadal
738 climate oscillation with impacts on salmon, Bull. Amer. Meteor. Soc., 78, 1069–1079, 1997.
739
740 Mart, Y.: The tectonic setting of the Seychelles, Mascarene and Amirante plateaus in the
741 Western Equatorial Indian ocean, Marine Geology, 79, 261-274, 1988.
742
743 McGregor H. V. and Gagan M. K.: Diagenesis and geochemistry of Porites corals from Papua
744 New Guinea: implications for paleoclimate reconstruction, Geochim. Cosmochim. Acta, 67,
745 2147–2156, 2003.

McGregor, H. V. and Abram, N. J.: Images of diagenetic textures in Porites corals from Papua New Guinea and Indonesia, Geochemistry, Geophysics, Geosystems 9(10), doi:10.1029/2008GC002093, 2008.

McPhaden, M. J., Zebiak, S. E., Glantz, M. H.: ENSO as an Integrating Concept in Earth Science, Science, 314, 1740-1745, 2006.

Meehl, G. A., and Hu, A.: Megadroughts in the Indian Monsoon Region and Southwest North America and a mechanism for associated Multidecadal Pacific Sea Surface Temperature Anomalies, J. Climate, 19, 1605-1623, 2006.

Nakamura, N., Kayanne, H., Iijima, H., McClanahan, T. R., Behera, S. K. and Yamagata, T.: Mode shift in the Indian Ocean climate under global warming stress, Geophysical Research Letters, 36, L23708, doi:10.1029/2009GL040590, 2009.

New A. L., Alderson S. G., Smeed D.A., Stansfield K.L.: On the circulation of water masses across the Mascarene Plateau in the South Indian Ocean, *Deep-Sea Research I* 54, 42–74, 2007.

New A. L., Stansfield, K., Smythe-Wright, D., Smeed D. A., Evans, A. J. and Alderson, S. G.: Physical and biochemical aspects of the flow across the, Mascarene Plateau in the Indian Ocean, *Philosophical Transactions of the Royal Academic Society* 363, 151–168, 2005.

Nurhati, I. S., Cobb, K. M. and Lorenzo E. D. Decadal-Scale SST and Salinity Variations in the Central Tropical Pacific: Signatures of Natural and Anthropogenic Climate Change. Journal of Climate 24: 3294-3308, 2011.

Paillard, D., Labeyrie, L., Yiou, P.: Macintosh program performs time series analysis. Eos Trans AGU 77, 379, 1996.

776 Pfeiffer, M., Timm, O. and Dullo, W.-C.: Oceanic forcing of interannual and multidecadal
777 climate variability in the southwestern Indian Ocean: Evidence from a 160 year coral isotopic
778 record (La Reunion, 50E, 21S). Paleoceanography, 19, PA4006, doi:10.1029/2003PA000964,
779 2004.
780

781 Pfeiffer M. and Dullo, W.-Ch. Monsoon-induced cooling of the western equatorial Indian
782 Ocean as recorded in coral oxygen isotopes records from the Seychelles covering the period
783 1840-1994 AD. Quat Sci Rev 25:993–1009, 2006.

784

785 Pfeiffer, M., Dullo, W.-C., Zinke, J. and Garbe-Schoenberg, D.: Three monthly coral Sr/Ca
786 records from the Chagos Archipelago covering the period of 1950-1995 A.D.: reproducibility
787 and implications for quantitative reconstructions of sea surface temperature variations,
788 International Journal of Earth Sciences, 98, doi:10.007/s00531-00008-00326-z, 2009.
789

790 Rayner, N. A., Parker, D. E., Horton, E. B., Folland, C. K., Alexander, L. V., Rowell, D. P.,
791 Kent, E. C. and Kaplan A.: Global analyses of sea surface temperature, sea ice, and night
792 marine air temperature since the late nineteenth century. Journal of Geophysical Research
793 108(D14), doi:10.1029/2002JD002670, 2003.
794

795 Reason, C.J.C. Subtropical Indian Ocean SST dipole events and southern African rainfall,
796 Geophys. Res. Lett., 28 (11) 2225–2227, 2001.
797

798 Reynolds, R.W., Rayner, N.A., Smith, T.M., Stokes, D.C., Wang W.: An improved in situ and
799 satellite SST analysis for climate, Journal of Climate, 15, 1609–1625, 2002.
800

801 Reynolds, R. W., Smith, T. M., Liu, C., Chelton, D. B., Casey, K. S. and Schlax, M. G.: Daily
802 high-resolution blended analyses for sea surface temperature, J. of Climate, 20, 5473-5496,
803 2007.
804

805 Sayani, H. R., Cobb, K. M., Cohen, A. L., Crawford Elliott, W., Nurhati, I. S., Dunbar, R. B.,
806 Rose, K. A., Zaunbrecher, L. K.: Effects of diagenesis on paleoclimate reconstructions from
807 modern and young fossil corals, Geochimica et Cosmochimica Acta, 75, 6361–6373, 2011.
808
809 Schott, F.A., McCreary, J.P.: The monsoon circulation of the Indian Ocean, Progress in
810 Oceanography, 51, 1–123, 2001.
811
812 Schrag, D.P.: Rapid analyses of high-precision Sr/Ca ratios in corals and other marine
813 carbonates, Paleoceanography, 14, 2, 97-102, 1999.
814
815 Sheppard, C.R.C. Predicted recurrences of mass coral mortality in the Indian Ocean.
816 Nature, 425, 294-297, 2003.
817
818 Smith, T.M., Reynolds, R.W., Peterson, T.C., Lawrimore, J.: Improvements to NOAA's
819 historical merged land–ocean surface temperature analysis (1880–2006), J. of Climate, 21,
820 2283, 2008.
821
822 Smodej, J., Reuning, L., Wollenberg, U., Zinke, J., Pfeiffer, M. and Kukla, P. A.: Two-
823 dimensional X-ray diffraction as a tool for the rapid, nondestructive detection of low calcite
824 quantities in aragonitic corals, Geochemistry, Geophysics, Geosystems, 16,
825 10.1002/2015GC006009, 2015.
826
827 Tokinaga, H., Xie, S.P., Deser, C., Kosaka, Y., Okumura, Y. M.: Slowdown of the
828 Walker circulation driven by tropical Indo-Pacific warming. Nature, 491, 439-444, 2012.
829
830 Trouet, V. and van Oldenborgh, G.J. KNMI Climate Explorer: a web-based research tool
831 for high-resolution paleoclimatology. Tree Ring Research, 69, 1, 3-13 (2013).
832
833 Turner, J. and Klaus, R.: Coral reefs of the Mascarenes, Western Indian Ocean, Philosophical
834 transactions of the Royal Academic Society, 363, 229–250, 2005.

van Oldenborgh, G. J., Burgers, G.: Searching for decadal variations in ENSO precipitation teleconnections, Geophys. Res. Lett., 32, L15701, 2005.

Woodruff, S.D. *et al.*: ICOADS Release 2.5: Extensions and enhancements to the surface marine meteorological archive, Int. J. Climatol., 31, 951-967, 2011.

Xie, S.-P., Kosaka Y., Du Y., Hu K. M., Chowdary J. S., and Huang G.: Indo-western Pacific ocean capacitor and coherent climate anomalies in post-ENSO summer: A review, Adv. Atmos. Sci., 33(4), 411–432, 2016.

Zinke, J., Pfeiffer, M., Park, W., Schneider, B., Reuning, L., Dullo, W.-Chr., Camoin, G. F., Mangini, A., Schroeder-Ritzrau, A., Garbe-Schönberg, D. and Davies, G. R.: Seychelles coral record of changes in sea surface temperature bimodality in the western Indian Ocean from the Mid-Holocene to the present, Climate Dynamics, 43 (3), 689-708, 2014.

Zinke, J., Pfeiffer, M., Timm, O., Dullo, W.-Chr. and Brummer, G. J. A. Western Indian Ocean marine and terrestrial records of climate variability: a review and new concepts on land-ocean interaction since A.D. 1660. International Journal of Earth Sciences 98, Special Volume. doi:10.007/s00531-008-0365-5, 2009.

Zinke, J., Timm, O., Pfeiffer, M., Dullo, W.-Chr., Kroon, D. and Thomassin, B. A. Mayotte coral reveales hydrological changes in the western Indian between 1865 to 1994. Geophysical Research Letters 35, L23707, doi:10.1029/2008GL035634, 2008.

Zinke, J., Dullo, W.-Chr., Heiss, G. A. & Eisenhauer, A. ENSO and subtropical dipole variability is recorded in a coral record off southwest Madagascar for the period 1659 to 1995. Earth and Planetary Science Letters 228 (1-2), 177-197, 2004.

Tables

Core name	GPS position	Species	Water depth (m)	Mean growth rate mm year^{-1}	Mean density g/cm^3	Mean Calcification rate g/cm^2 year^{-1}
Totor	S19º40.237; E63º25.754	*Porites sp.*	4.0	9.2 (±0.19)	1.128 (±0.11)	1.07 (±0.18)
Cabri	S19°40.030, E63°26.065	*Porites lobata*	3.0	11.8 (±0.25)	1.36 (±0.12)	1.60 (±0.16)

Table 1 - Coral cores with their GPS co-ordinates and colony depths at low tide, with mean rates of extension, density and calcification over the complete length of the individual records (1907 to 2006 for Cabri; 1781 to 2005 for Totor).

Section	Year	Orientation	Bias	Notes
1	2005-1987	Sub-optimal	cool	Corallites parallel to surface, yet straight angle; probably like a valley
2	1987-1982	Sub-optimal	cool	Corallites parallel to surface, yet straight angle; probably like a valley
2	**1981-1977**	**Sub-optimal**	**none**	**Corallites at an angle to the surface; no bias**
3	**1978-1975**	**Sub-optimal**	**none**	**Corallites at an angle to the surface; no bias**
3	**1974-1958**	**Optimal**	**none**	**Corallites parallel to surface; no bias**
4A	1958-1952	Sub-optimal	warm	Corallites at an angle to the surface; scallop texture from angles of corallites
4A	1951-1945	Sub-optimal	warm	Corallites at an angle to the surface; 1947-1952 low growth rate; reduced seasonality
4B	**1947-1936**	**Optimal**	**none**	**Corallites parallel to surface, 1945-1947 better orientation than in slab 4A**
4B	**1938-1933**	**Sub-optimal**	**none**	**Corallites at an angle to the surface; 1936-1941 warm anomaly years show normal seasonality and high growth rate**
5	**1933-1922**	**Optimal**	**none**	**Corallites parallel to surface; 1922-1928 reduced seasonality**
6	1921-1915	Sub-optimal	warm	1915-21 warm spikes shows slightly oblong corallites, yet normal seasonality; switch from optimal to sub-optimal orientation
6	**1915-1896**	**Optimal to Sub-optimal**	**none**	**Corallites mostly parallel to surface, small section with corallites at slight angle;;**
7	**1897-1890**	**Optimal**	**none**	**Corallites parallel to surface**
7	1887-1882	Optimal	cool	Diagenesis detected between years 1882-1887
7	**1881-1872**	**Sub-optimal**	**none**	**Corallites at an angle to the surface; 1872 close to bioerosion track; 1878-1880 low seasonality, yet no effect**
8	1872-1868	Sub-optimal	cool	Corallites at an angle to the surface; some corallites at almost 90° angle; 1868-1872 below bioerosion track; 1867-1871 low seasonality
9	1860-1854	Sub-optimal	warm	Corallites at an angle to the surface; 1854-1858 low seasonality, less winter samples
9	1856-1845	Sub-optimal	warm	Corallites parallel to surface; low seasonality with relatively warm winter samples
9	**1844-1831**	**Optimal**	**none**	**Corallites parallel to surface; only 1831-1832 corallites at an angle to surface**
10	1830-1827	Sub-optimal	warm	Corallites at an angle to the surface; oblong orientation
10	1826-1823	Disorganised	warm	Corallites rotating at 90° angle; low growth rate, seasonality reduced 1823-1825 with relatively warm winter samples
10	**1822-1815**	**Optimal**	**none**	**Corallites parallel to surface; low growth rate; reduced seasonality 1818-1822, yet no effect on SST anomalies**
11	**1816-1806**	**Sub-optimal**	**none**	**Corallites at an angle to the surface, yet no effect on SST anomalies**
11	**1807-1798**	**Sub-optimal**	**none**	**Corallites at an angle to the surface in sub-optimal parts; Corallites rotating at 90° angle near terminating fans (not sampled); 3 growth axes with terminating fans in between (not sampled); 1799-1807 regular seasonality**
11	1797-1792	Sub-optimal	warm	Corallites at an angle to the surface
12	1795-1792	Disorganised	warm	Corallites rotating at 90° angle; 1792-1791 long year, more summer samples
12	1791-1784	Sub-optimal	warm	Corallites parallel to surface; 1784-1787 Corallites at an angle to the surface; 1789-1794 seasonality distorted
12	1781-1783	Disorganised	warm	Corallites rotating at 90° angle; seasonality slightly distorted, apparently more summer samples

883 Table 2 – Summary of sampling issues detected in core Totor. Unbiased sampling tracks
884 indicated in bold.

Section	Year	Orientation	Bias	Notes
1	2007-2000	Sub-optimal	warm	Corallites parallel to surface; yet no clear growth fans
1	**1999-1992**	**Optimal**	**none**	**Corallites parallel to surface**
2	**1984-1992**	**Sub-optimal**	**none**	**Corallites at an angle to the surface; oblong corallites**
3	**1983-1968**	**Sub-optimal**	**none**	**Corallites parallel to surface; yet no clear growth fan**
4	**1967-1964**	**Sub-optimal**	**none**	**Corallites at an angle to the surface**
5	**1963-1958**	**Optimal**	**none**	**Corallites parallel to surface**
5	**1957-1954**	**Sub-optimal**	**none**	**Corallites at an angle to the surface**
5	**1953-1945**	**Optimal**	**none**	**Corallites parallel to surface**

885
886 Table 3 – Summary of sampling issues detected in core Cabri. Unbiased sampling tracks
887 indicated in bold.
888

889 **Figure captions**

890 Figure 1 – a) Map of Rodrigues Island with the position of the two corals cores at Totor
891 and Cabri indicated. The star shows the position of the CTD that collects SST and salinity
892 data. Polygon indicates the location of the Meteorological Station which records air
893 temperature, sunshine hours, wind speed and rainfall. b) Spatial correlation between
894 January-March averaged SIOD index (Behera and Yamagata, 2001) with HadISST for
895 Rodrigues Island (Rayner et al., 2003). c) Spatial correlation between July-June mean
896 annual averaged PDO index (Mantua et al., 1997) with HadISST (Rayner et al., 2003).
897 All correlations with detrended data. Only correlation with $p<0.05$ are coloured.
898 Computed at KNMI climate explorer (van Oldenborgh and Burgers, 2005). Yellow star in
899 b) and c) marks the location of Rodrigues Island.
900

901 Figure 2 – a) Time series of monthly (thin solid lines) Sr/Ca anomalies (right Y-axis
902 converted) relative to the 1961 to 1990 climatological mean for coral cores Cabri (top),
903 Totor (middle) for the period 1781 to 2006. Annual mean time series of individual cores
904 (red line) b) Cabri and c) Totor compared to SST reconstructions: ERSSTv3b, ERSSTv4,
905 HadISST, HadSST3, HadMAT1 and HadNMAT2. See legend in b) and c) for colour

code. For all time series we computed anomalies relative to 1961 to 1990. The uncertainty of mean annual coral Sr/Ca-SST anomalies is indicated by the grey envelope. Potential warm bias in coral SST is indicated in parathenses, pointing up for warm and down for potential cool biases, respectively. Parathenses with inset D marks core interval with diagenesis.

Figure 3 - Thin-section and SEM images of primary coral aragonite (PA) and aragonite cement (AC) in cores Totor and Cabri. A and B: Excellent preservation of the primary coral aragonite in core section 4A and 4B in Totor. Trace amounts of aragonite cements occur as isolated patches in core sections 6 (C), 7 (D) and 11 (E) of Totor. F (left): A prominent growth break (stippled line) in core section 12 of Totor is encrusted by coralline red algae (CRA). F (middle): The section above the growth break shows well preserved primary coral aragonite. F (right): The pristine coral skeleton of core Cabri contains locally aragonitic sediment (S) partially filling growth-framework pores. A to E: Thin section photographs are shown in plane- (left) and cross-polarized light (middle). F: All thin section photographs are shown in plane-polarized light.

Figure 4 – a) Climatology at Rodrigues between 1997 to 2007. Monthly averaged SST *in situ* (red), ERSSTv.3b (grey; Smith et al., 2008) and AVHRR SST (blue stippled; Reynolds et al., 2007); b) Reconstructed absolute SST from coral Sr/Ca from cores Totor (dark grey with triangle) and Cabri (light grey with diamond) for 2002 to 2006 based on calibration with *in situ* SST from Rodrigues (red). The uncertainty for single month

928 absolute SST for individual cores Cabri and Totor is 1.23°C and 1.05°C (1σ),
929 respectively. The coral data agree with *in situ* SST within the 1σ uncertainty.
930
931 Figure 5 – Time series of annual mean temperatures anomalies relative to the 1961-1990
932 mean for the coral Cabri SST reconstruction, Rodrigues weather station air temperature
933 (AT), ERSSTv3b, ERSSTv4, HadISST, HadSST3, HadMAT1 and HadNMAT2 for the
934 period 1950 to 2006. The uncertainty of mean annual coral Sr/Ca-SST anomalies is
935 indicated by the grey envelope.
936
937 Figure 6 – Spatial correlation of Cabri Sr/Ca-SST anomalies (relative to 1961-1990) with
938 HadISST (Rayner et al., 2003). January to March austral summer in a) between 1945-
939 2006, b) 1961-1990 and c) 1971-2006. Annual mean correlations in d) between 1945-
940 2006, e) 1961-1990 and f) 1971-2006. Only correlation with $p<0.05$ is coloured.
941 Computed at KNMI climate explorer (van Oldenborgh and Burgers, 2005). Yellow star in
942 a) marks location of Rodrigues Island.
943
944 Figure 7 – Spatial correlations of Left) Cabri coral SST and Right) HadISST grid for
945 Rodrigues Island with global austral summer HadISST for a-c) 1950 to 1975 (February to
946 May) negative PDO phase (Mantua et al., 1997) and c-d) 1976 to 1999 (January to April)
947 positive PDO phase. Only correlations with $p<0.05$ coloured. Computed at KNMI climate
948 explorer (van Oldenborgh and Burgers, 2005). Yellow star in a) marks location of
949 Rodrigues Island.
950

951 Figure 8 – Comparison of Southwestern Indian Ocean (SWIO) coral records from St.
952 Marie Island (black; Grove et al., 2013) with the Cabri record from Rodrigues (red). A
953 SST time series for the grid-box in the SWIO averaged between 12-20°S and 50-63°E is
954 also illustrated (light blue). All time were annualized and converted to SST anomalies
955 relative to 1961-1990. The uncertainty of mean annual Cabri Sr/Ca-SST anomalies is
956 indicated by the grey envelope.
957
958 Figure 9 – a) Monthly interpolated Sr/Ca profiles for cores Cabri (red) and Totor (grey).
959 b) Images of core Totor (coloured blue) with orientation of corallites indicated. Years for
960 core sections indicated on coral slab and grey arrow points to major change in growth
961 pattern in Totor core top section around the years 1983/84.
962
963 Figure A1 – X-ray negative print for core sections of core Totor with sampling lines
964 indicated. Blue lines indicate high resolution sampling tracks. Yellow lines superimposed
965 on blue lines indicate sampling at annual resolution for other purposes. Start or end years
966 for each core section indicated.
967
968 Figure A2 - X-ray negative print for core sections of core Cabri with sampling lines
969 (milling holes) indicated. Start or end years for each core section indicated. Note the dead
970 surface before 1907 that is most probably related to a past coral bleaching event.
971

Figure A3 –Number of SST observations in the grid box surrounding Rodrigues in the ICOADS database. Note the extremely sparse observations even in recent years (van Oldenborgh and Burgers, 2005).

Figure A4 – Spatial correlations of mean annual HadMAT1 air temperature anomalies between 1945 to 2001 relative to 1961-1990 with a) HadISST for Rodrigues, and b) Cabri SST. Only correlations with $p<0.05$ coloured. Computed at KNMI climate explorer (van Oldenborgh and Burgers, 2005). Y-axis Latitude, X-axis Longitude.

Table A1 – Statistics of various sea surface temperature (SST) products and air temperature for Rodrigues with 1σ standard deviations in brackets for the period 2002 to 2006 (period with *in situ* SST data). STDV = 1σ standard deviation over all years. All units in °C.

Table A2 - Linear regression of coral Sr/Ca with a) *in situ* SST 2002-2005/6, b) ERSSTv.3 (Smith et al., 2008) 1997-2005/6, c) AVHRR SST NOAA Coral Reef watch data 2000-2005/6 and d) monthly Sr/Ca with AVHRR SST (Reynolds et al., 2007) for the period 1982 to 2005.

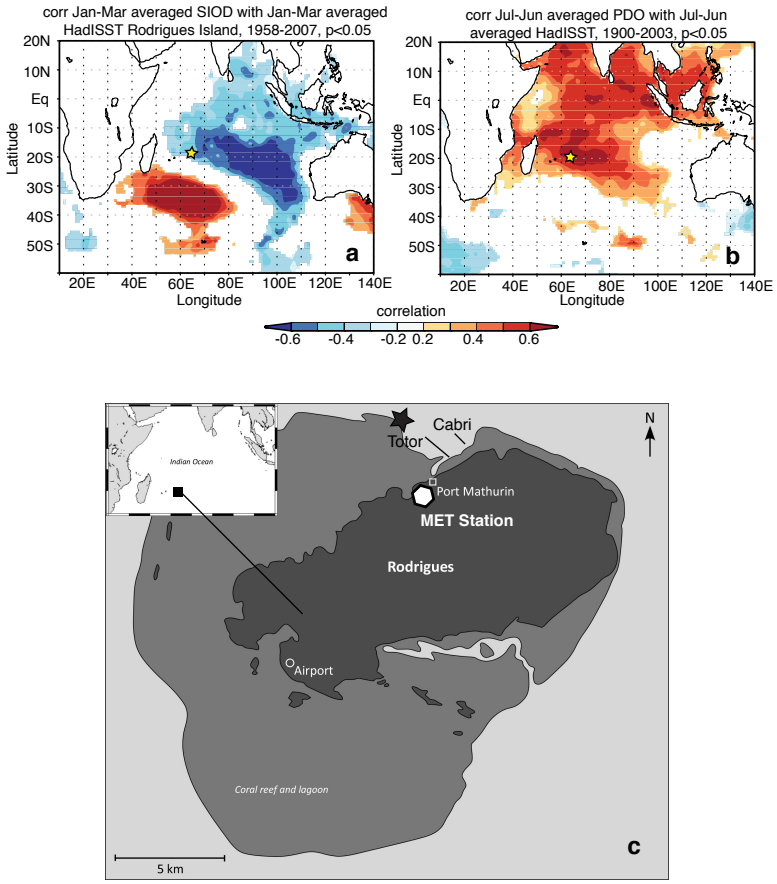

991

992 Figure 1 – a) Spatial correlation between January-March averaged SIOD index (Behera
993 and Yamagata, 2001) with HadISST (Rayner et al., 2003) for Rodrigues Island. b) Spatial
994 correlation between July-June mean annual averaged PDO index (Mantua et al., 1997)
995 with HadISST (Rayner et al., 2003). All correlations with detrended data. Only
996 correlation with $p<0.05$ are coloured. Computed at KNMI climate explorer (van
997 Oldenborgh and Burgers, 2005). Yellow star in a) and b) marks the location of Rodrigues
998 Island. c) Map of Rodrigues Island with the position of the two corals cores at Totor and
999 Cabri indicated. The star shows the position of the CTD that collects SST and salinity
1000 data. Polygon indicates the location of the Meteorological Station which records air
1001 temperature, sunshine hours, wind speed and rainfall.

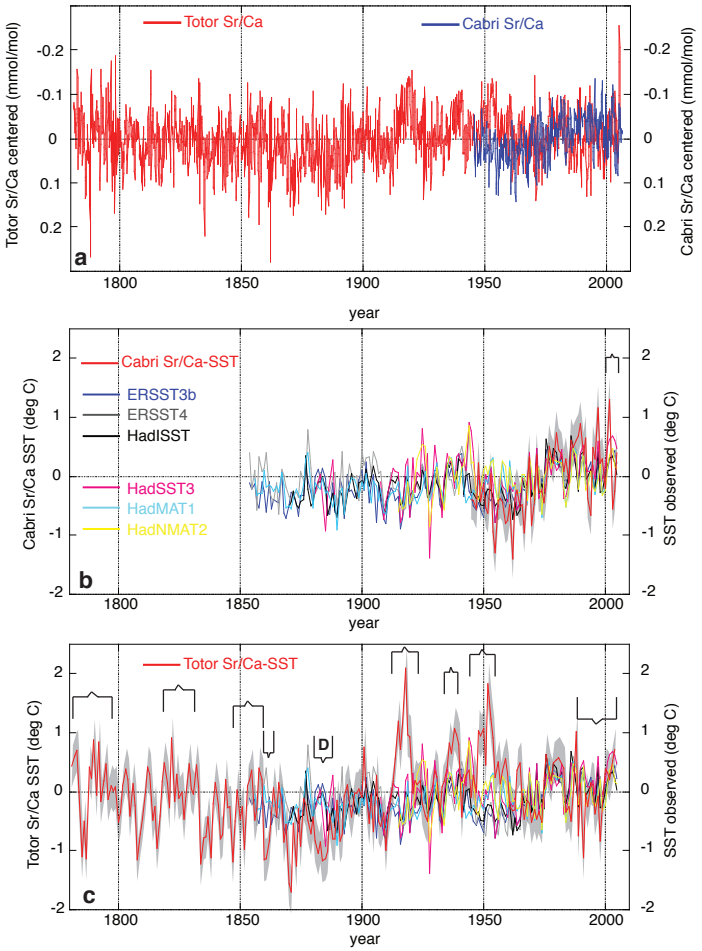

Figure 2 - a) Time series of monthly (thin solid lines) Sr/Ca anomalies (right Y-axis innverted) relative to the 1961 to 1990 climatological mean for coral cores Cabri (top), Totor (middle) for the period 1781 to 2006. Annual mean time series of individual cores (red line) b) Cabri and c) Totor compared to SST reconstructions: ERSSTv3b, ERSSTv4, HadISST, HadSST3, HadMAT1 and HadNMAT2. See legend in b) and c) for colour code. For all time series we computed anomalies relative to 1961 to 1990. The uncertainty of mean annual coral Sr/Ca-SST anomalies are indicated by the grey envelope. Potential warm bias in coral SST is indicated by brackets, pointing up for warm and down for potential cool biases, respectively. Bracket with inset D marks core interval with diagenesis.

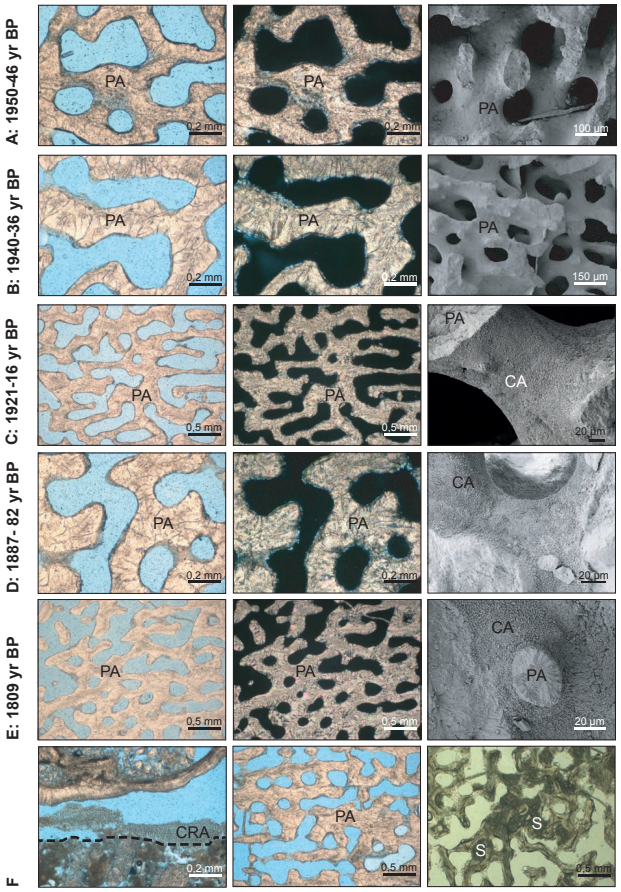

1014

1015 Figure 3 - Thin-section and SEM images of primary coral aragonite (PA) and aragonite
1016 cement (AC) in cores Totor and Cabri. A and B: Excellent preservation of the primary
1017 coral aragonite in core sections 4A and 4B in Totor. Trace amounts of aragonite cements
1018 occur as isolated patches in core sections 6 (C), 7 (D) and 11 (E) of Totor. F (left): A
1019 prominent growth break (stippled line) in core section 12 of Totor is encrusted by
1020 coralline red algae (CRA). F (middle): The section above the growth break shows well
1021 preserved primary coral aragonite. F (right): The pristine coral skeleton of core Cabri
1022 contains locally aragonitic sediment (S) partially filling growth-framework pores. A to E:
1023 Thin section photographs are shown in plane- (left) and cross-polarized light (middle). F:
1024 All thin section photographs are shown in plane-polarized light.

1025

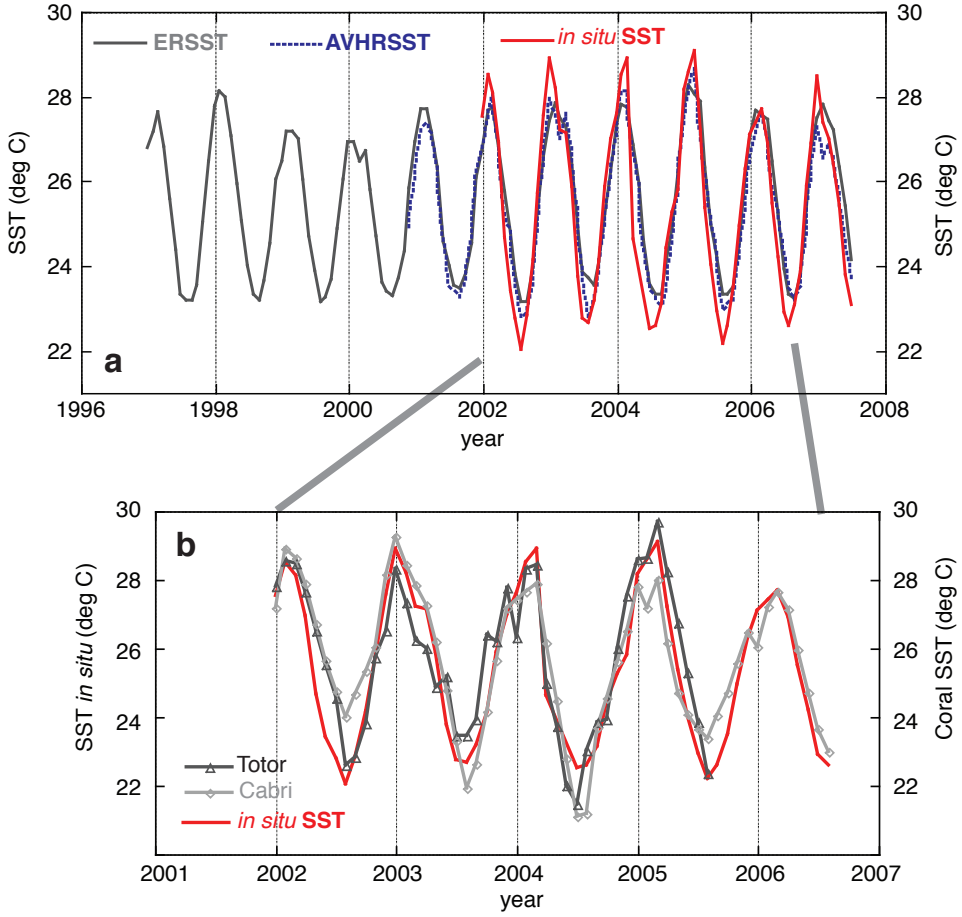

1026

1027 Figure 4 – – a) Climatology at Rodrigues between 1997 to 2007. Monthly averaged SST
1028 *in situ* (red), ERSSTv.3 (grey; Smith et al., 2008) and AVHRR SST (blue stippled;
1029 Reynolds et al., 2007); b) Reconstructed absolute SST from coral Sr/Ca from cores Totor
1030 (dark grey with triangle) and Cabri (light grey with diamond) for 2002 to 2006 based on
1031 calibration with in situ SST from Rodrigues (red). The uncertainty for single month
1032 absolute SST for individual cores Cabri and Totor is 1.23°C and 1.05°C (1σ),
1033 respectively. The coral data agree with *in situ* SST within the 1σ uncertainty.

1034

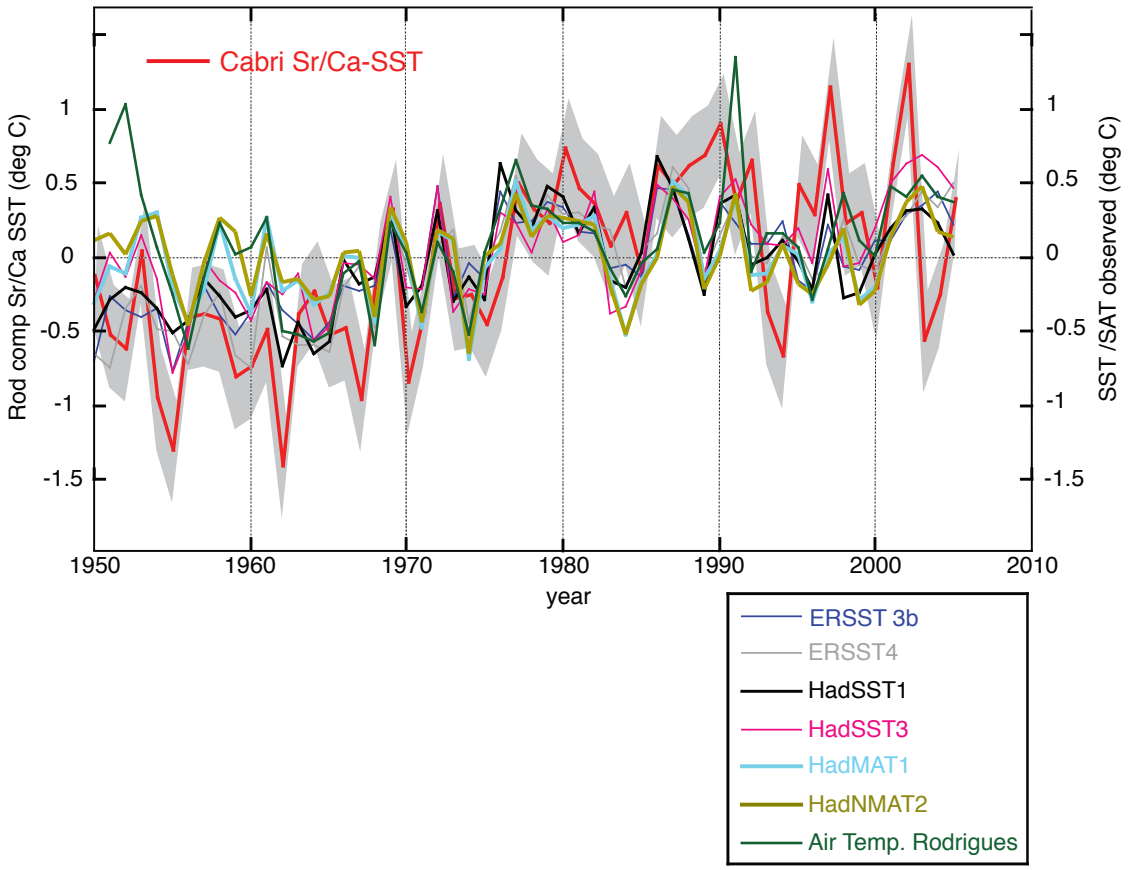

1035

1036 Figure 5 – Time series of annual mean temperatures anomalies relative to the 1961-1990
1037 mean for the coral Cabri SST reconstruction, Rodrigues weather station Air temperature
1038 (AT), ERSSTv3b, ERSSTv4 , HadISST, HadSST3, HadMAT1 and HadNMAT2 for the
1039 period 1950 to 2006. The uncertainty of mean annual coral Sr/Ca-SST anomalies are
1040 indicated by the grey envelope.

1041

1042

1043

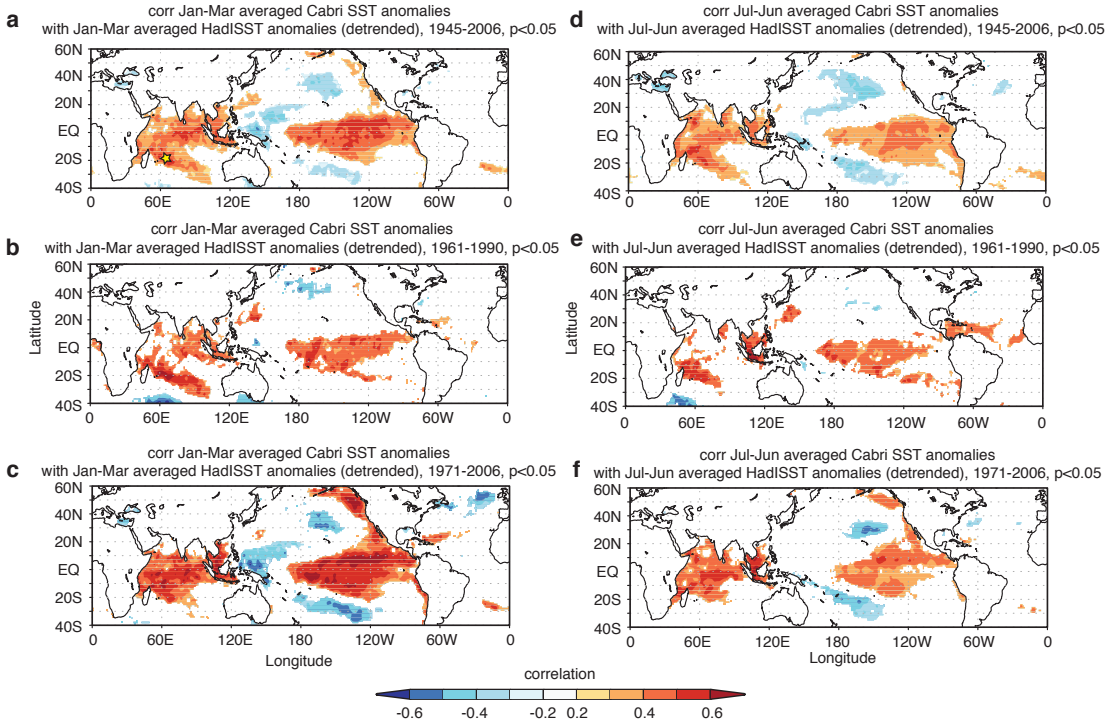

Figure 6 – Spatial correlation of Cabri Sr/Ca-SST anomalies (relative to 1961-1990) with HadISST (Rayner et al., 2003). January to March austral summer in a) between 1945-2006, b) 1961-1990 and c) 1971-2006. Annual mean correlations in d) between 1945-2006, e) 1961-1990 and f) 1971-2006. Only correlation with $p<0.05$ are coloured. Computed at knmi climate explorer (van Oldenborgh and Burgers, 2005). Yellow star in a) marks location of Rodrigues Island.

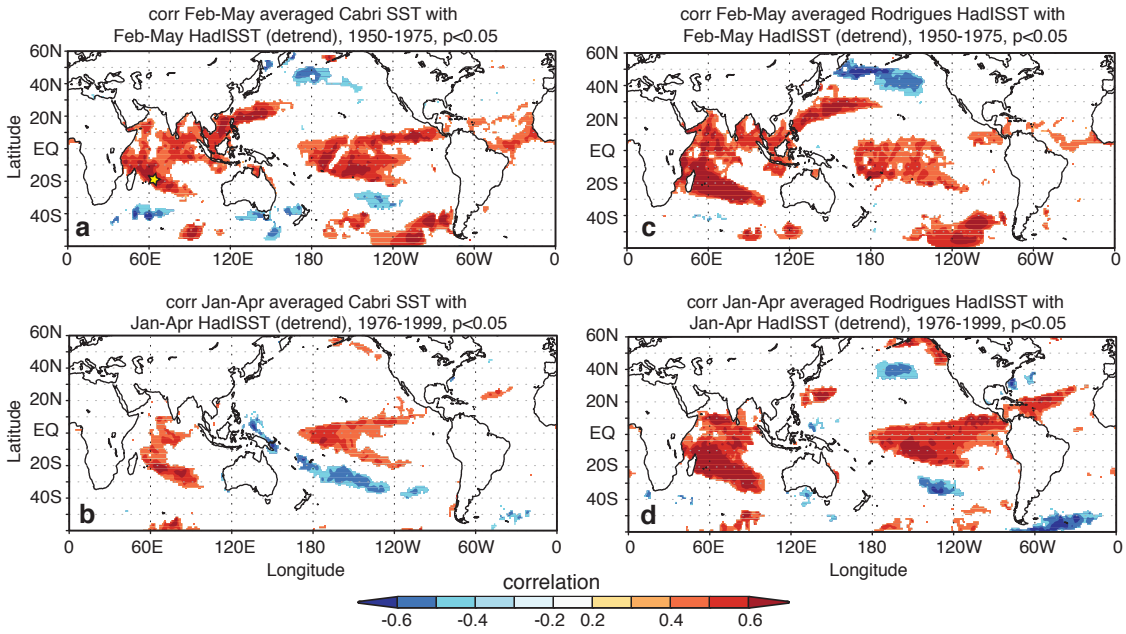

1053

1054 Figure 7 – Spatial correlations of Left) Cabri coral SST and Right) HadISST grid for
1055 Rodrigues Island with global austral summer HadISST for a-c) 1950 to 1975 (February to
1056 May) negative PDO phase (Mantua et al., 1997) and c-d) 1976 to 1999 (January to April)
1057 positive PDO phase. Only correlations with $p<0.05$ coloured. Computed at knmi climate
1058 explorer (van Oldenborgh and Burgers, 2005). Yellow star in a) marks location of
1059 Rodrigues Island.

1060

1061

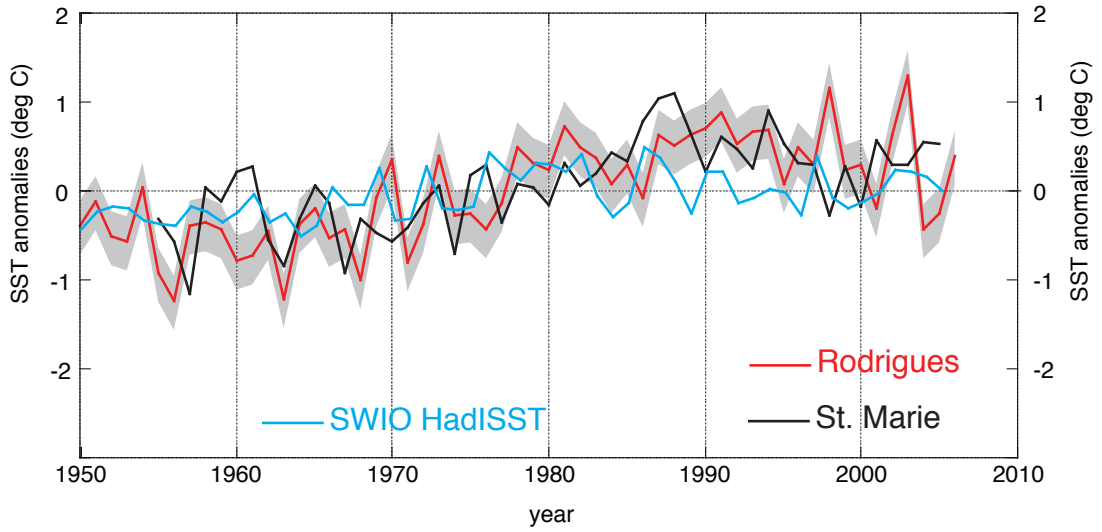

1062

1063 Figure 8 – Comparison of southwestern Indian Ocean (SWIO) coral records from St.
1064 Marie Island (black; Grove et al., 2013) with the Cabri record from Rodrigues (red). An
1065 SST time series for the grid-box in the SWIO averaged between 12-20°S and 50-63°E is
1066 also illustrated (light blue). All time were annualized and converted to SST anomalies
1067 relative to 1961-1990. The uncertainty of mean annual Cabri Sr/Ca-SST anomalies are
1068 indicated by the grey envelope.

1069

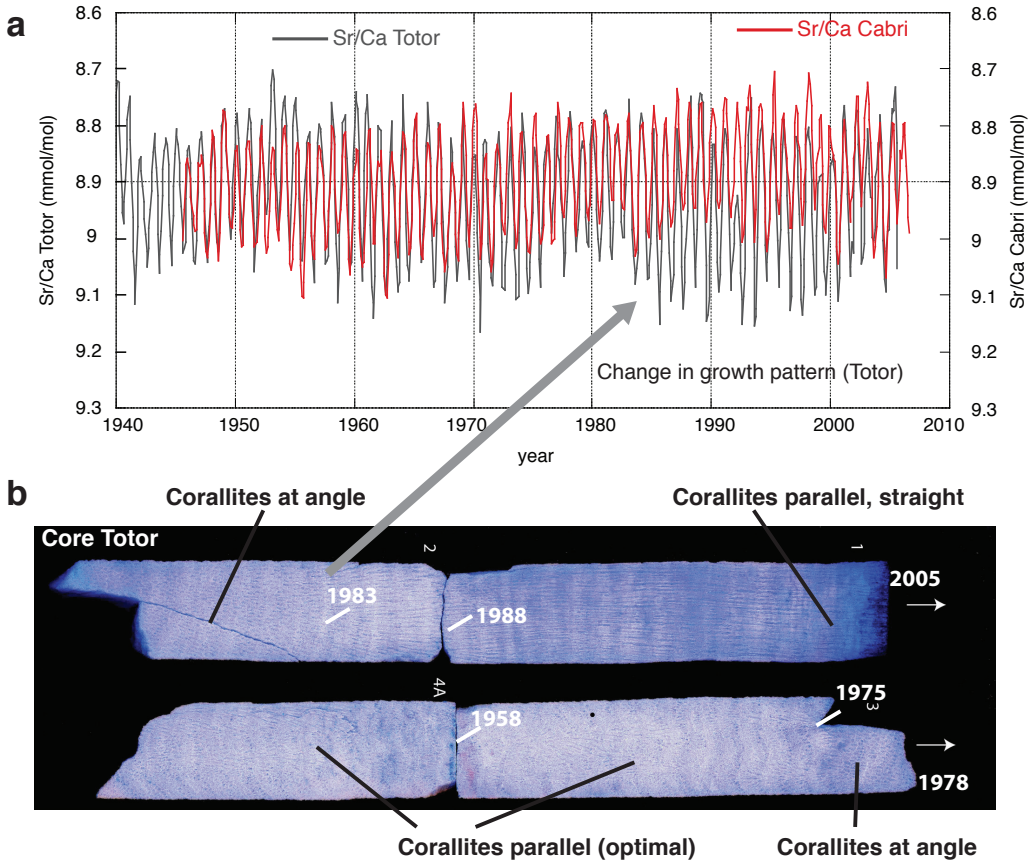

1070

1071 Figure 9 – a) Monthly interpolated Sr/Ca profiles for cores Cabri (red) and Totor (grey).
1072 B) Images of core Totor (coloured blue) with orientation of corallites indicated. Years for
1073 core sections indicated on coral slab and grey arrow points to major change in orientation
1074 of corallites in core top section of Totor around 1983/84.

1075

1076

1077

1078

1079

1080

1081

Appendix A –Instrumental sea surface temperature (SST) records and linear regression equations of coral Sr/Ca with SST.

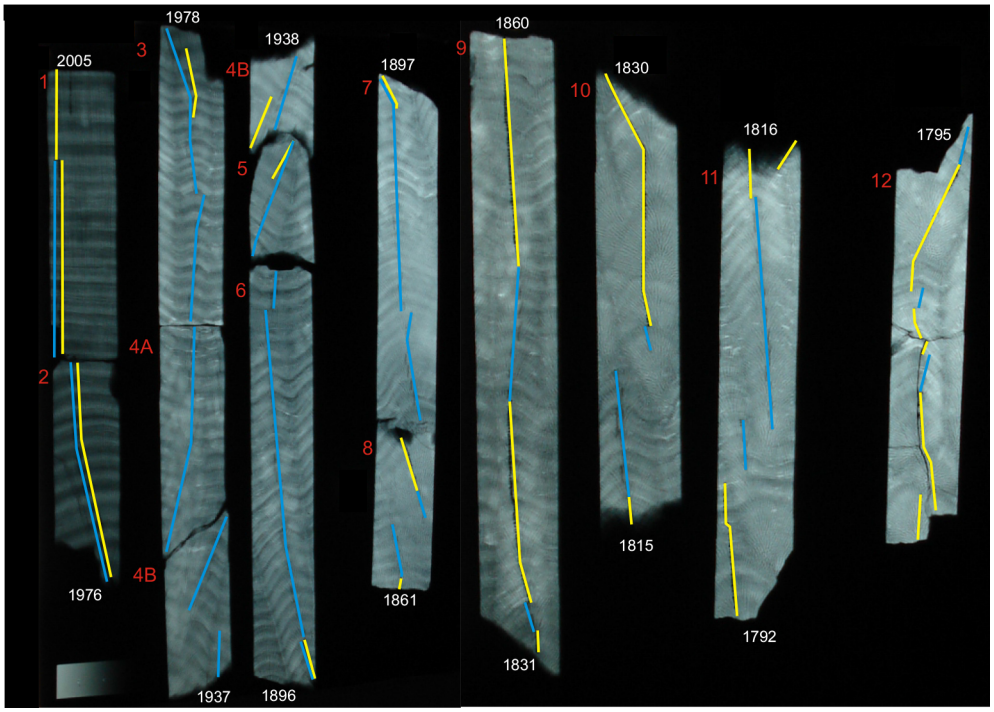

Figure A1 – X-ray negative print for core sections of core Totor with sampling lines indicated. Blue lines indicate high resolution sampling tracks. Yellow lines superimposed on blue lines indicate sampling at annual resolution for other purposes. Start or end years for each core section indicated.

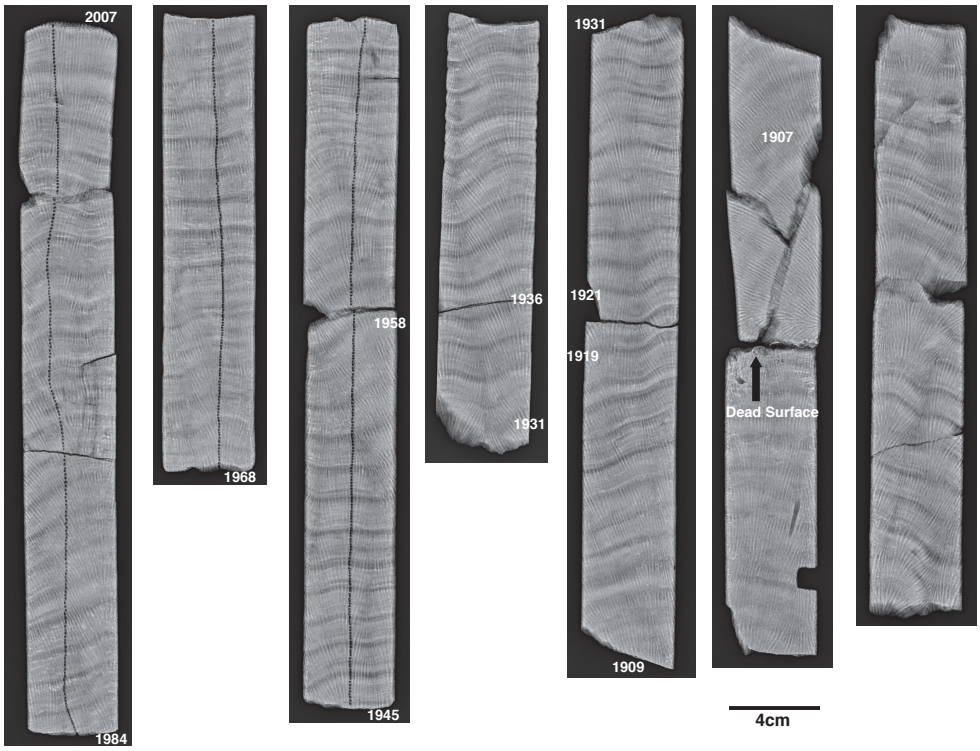

Figure A2 - X-ray negative print for core sections of core Cabri with sampling lines (milling holes) indicated. Start or end years for each core section indicated. Note the dead surface before 1907 that is most probably related to a past coral bleaching event.

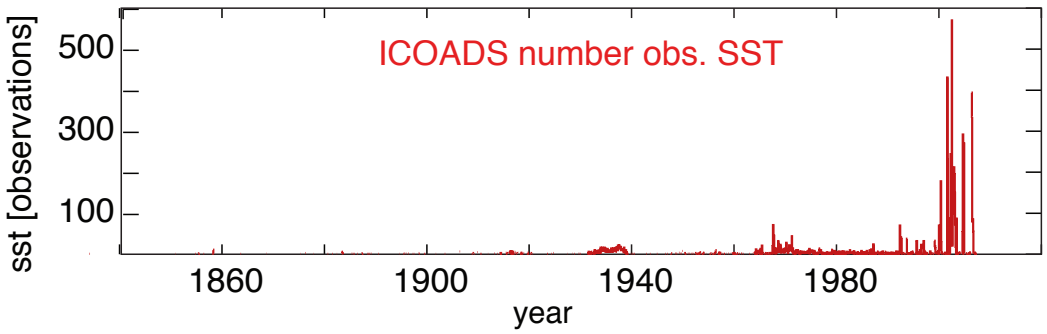

1099

1100 Figure A3 –Number of SST observations in the grid box surrounding Rodrigues in the
1101 ICOADS database. Note the extremely sparse observations even in recent years (van
1102 Oldenborgh and Burgers, 2005).

1103

1104

1105

1106

1107

1108

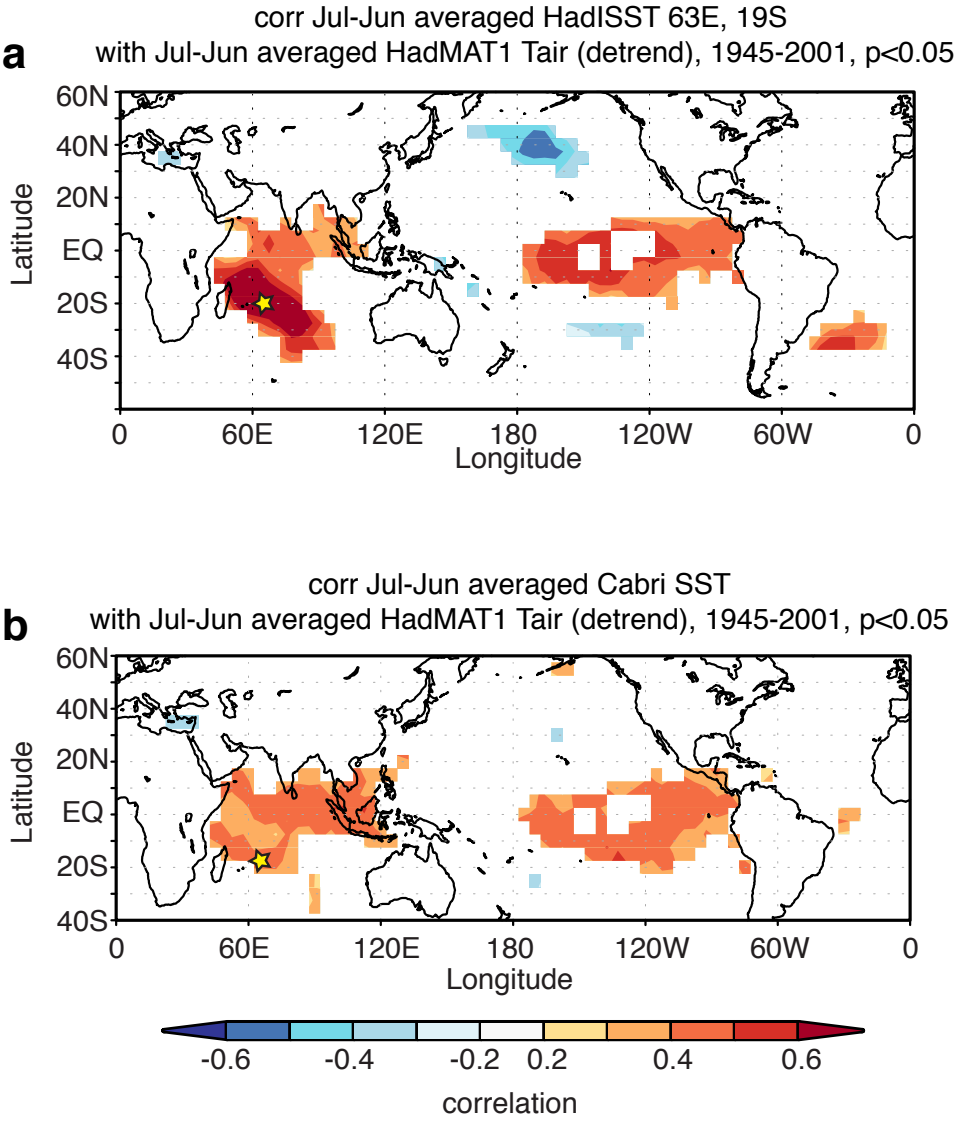

1109

1110 Figure A4 – a) Spatial correlation of HadISST for the grid box of Rodrigues Island with
1111 global HadMAT1 marine air temperature (Tair) between 1945 and 2001 for July to June
1112 annual averages (Rayner et al., 2003). Note the location of Rodrigues Island marked by
1113 yellow star. b) same as a), but for Cabri SST with global HadMAT1. Only correlations
1114 with p<0.05 coloured. Computed at knmi climate explorer (van Oldenborgh and Burgers,
1115 2005).

1116

1117

	SST *in situ* 2002-2006	**AVHRR SST 2002-2006**	**ERSST 2002-2006**	**Air Temp. 2002-2006**
Mean annual	25.49 (0.24)	25.4 (0.11)	25.57 (0.3)	27.49 (0.31)
Maximum	28.6 (0.5)	28.65 (0.44)	28.29 (0.4)	31.2 (0.62)
Minimum	22.4 (0.27)	22.75 (0.21)	23.15 (0.13)	24.2 (0.44)
Seasonal Range	6.22 (0.68)	5.9 (0.58)	5.14 (0.39)	7.0 (0.79)
STDV	2.14	1.78	1.69	2.07

1118

1119 Table A1 – Statistics of various sea surface temperature (SST) products and air
1120 temperature for Rodrigues with 1σ standard deviations in brackets for the period 2002 to
1121 2006 (period with *in situ* SST data). STDV = 1σ standard deviation over all years. All
1122 units in °C.

1123

1124

1125

1126

1127

1128

1129

1130

1131

1132

1133

(a) Max-Min	Regression equation	r^2	p
Totor	Sr/Ca = -0.0439(±0.004)*SST + 10.032(±0.10)	0.97	<0.001
Cabri	Sr/Ca = -0.0384(±0.005)*SST + 9.861(±0.12)	0.89	<0.001
(b) Max-Min			
Totor	Sr/Ca = -0.0638(±0.004)*SST + 10.566(±0.09)	0.95	<0.001
Cabri	Sr/Ca = -0.0507(±0.004)*SST + 10.179(±0.10)	0.90	<0.001
(c) Max-Min			
Totor	Sr/Ca = -0.0531(±0.004)*SST + 10.271(±0.11)	0.96	<0.001
Cabri	Sr/Ca = -0.0441(±0.005)*SST + 10.012(±0.13)	0.88	<0.001
(d) Monthly			
Totor	Sr/Ca = -0.0522(±0.003)*SST + 10.272(±0.08)	0.79	<0.001
Cabri	Sr/Ca = -0.0419(±0.003)*SST + 9.95(±0.07)	0.87	<0.001

Table A2 - Linear regression of coral Sr/Ca with a) *in situ* SST 2002-2005/6, b) ERSSTv.3 (Smith et al., 2008) 1997-2005/6, c) AVHRR SST NOAA Coral Reef watch data 2000-2005/6 and d) monthly Sr/Ca with AVHRR SST (Reynolds et al., 2007) for the period 1982 to 2005.